Rapid nongenomic estrogen signaling controls alcohol drinking behavior

Lia J. Zallar[1], Jean K. Rivera-Irizarry[2], Peter U. Hamor[3], Irena Pigulevskiy[1], Ana-Sofia Rico Rozo[3], Hajar Mehanna[3], Dezhi Liu[3], Jacqueline P. Welday[2], Rebecca Bender[3], Joseph J. Asfouri[3], Olivia B. Levine[2], Mary Jane Skelly[3†], Colleen K. Hadley[5], Kristopher M. Fecteau[4], Scottie Nelson[3], John Miller[3], Pasha Ghazal[3‡], Peter Bellotti[3], Ashna Singh[2], Lauren V. Hollmer[1], David W. Erikson[4], Jacob Geri[3], Kristen E. Pleil[1,2,3*]

[1]Pharmacology Graduate Program, Weill Cornell Graduate School of Medical Sciences, Weill Cornell Medicine, Cornell University, New York, NY, USA
[2]Neuroscience Graduate Program, Weill Cornell Graduate School of Medical Sciences, Weill Cornell Medicine, Cornell University, New York, NY, USA
[3]Department of Pharmacology, Weill Cornell Medicine, Cornell University, New York, NY, USA
[4]Endocrine Technologies Core, Oregon National Primate Research Center, Beaverton, OR, USA
[5]Weill Cornell/Rockefeller/Sloan Kettering Tri-institutional MD-PhD Program, New York, NY 10065, USA.
†Current affiliation: Psychology Department, Iona University, New Rochelle, NY, USA
‡Current affiliation: Department of Biosciences, COMSATS University Islamabad (CUI), Islamabad, Pakistan
*correspondence can be directed to krp2013@med.cornell.edu

Abstract

Ovarian-derived estrogen is a key modulator of numerous physiological processes via genomic and nongenomic mechanisms, including signaling non-canonically at membrane-associated estrogen receptors in the brain to rapidly regulate neuronal function. However, the mechanisms mediating estrogen regulation of behaviors such as alcohol consumption remain unclear. Early alcohol drinking confers greater risk for alcohol use disorder in women than men, and binge alcohol drinking is correlated with high circulating estrogen levels, but a causal role for estrogen signaling in driving alcohol drinking in gonadally-intact animals has not been established. We found that female mice displayed greater binge alcohol drinking and reduced avoidance behavior when circulating estrogen was high during the proestrus phase of the estrous cycle than when it was low, contributing to sex differences in these behaviors. The pro-drinking, but not anxiolytic, effect of high endogenous estrogen state occurred via rapid estrogen signaling at membrane-associated estrogen receptor alpha in the bed nucleus of the stria terminalis, which promoted synaptic excitation of corticotropin-releasing factor neurons and facilitated their activity during alcohol drinking behavior. This study is the first to demonstrate a rapid, nongenomic signaling mechanism for ovarian-derived estrogen signaling in the brain controlling behavior in gonadally intact females, and it establishes a causal role for estrogen in an intact hormonal context for driving alcohol consumption that contributes to known sex differences in this behavior.

Introduction

Sex is a major regulator of behavior across species, but the numerous underlying neurobiological mechanisms that mediate these differences are not fully characterized[1]. One critical neuromodulator of behavior is the sex steroid hormone estrogen (17β-estradiol; E2), which is produced in high volumes in the ovaries of females during the menstrual cycle in humans and estrous cycle in rodents[2]. E2 signaling is critical for the maintenance of numerous adaptive behaviors in both sexes, such as reproduction[3], learning and memory[4,5], and emotional behaviors[6], but it may also support maladaptive behaviors related to neuropsychiatric diseases[7-9]. E2 has been classically described to affect behavior through its engagement with nuclear estrogen receptors (ERs) to produce broad transcriptional changes via genomic mechanisms[1]. However, it can also act at membrane-associated ERs in the brain to rapidly modulate synaptic transmission and intrinsic excitability in brain regions including the hippocampus, hypothalamus, striatum, nucleus accumbens, and amygdala[5,10-16].

While a rapid signaling mechanism has been less explored for its role in E2 regulation of behavior, work in ovariectomized female rodents has established that E2 signals at membrane-associated ERs in the hippocampus to promote memory consolidation important for later recall using a modified E2 that is cell membrane-impermeable and thus can only signal at receptors at the membrane[17]. And, a host of research has demonstrated that E2 can rapidly modulate behavior in gonadectomized rodents, implicating but not directly showing a rapid, membrane signaling mechanism. For example, acute administration of E2 or ER modulators can regulate behaviors including aggression[18,19] and reproductive/sexual behavior[20] in castrated male rodents, as well as learning and memory[21,22] and psychostimulant self-administration/hyperlocomotion in ovariectomized female rodents[23-25]. In gonadally-intact males, pioneering work in birds has established that E2 (aromatized locally in birdsong brain regions from gonadal testosterone) rapidly regulates neuronal function to mediate birdsong and reproductive behaviors[26-30]; and, acute bioavailability of E2 is needed for male sexual behavior in intact male rodents[27,31]. Endogenous, ovarian-derived E2 may also be able to signal rapidly in the female brain to control behavior, but this has yet to be explored in gonadally-intact animals.

There is significant evidence that E2 is a key neuromodulator driving alcohol and drug-related behaviors[8,32-35], including excessive alcohol consumption and anxiety[9,35-37] that are primary risk factors for numerous psychiatric diseases including alcohol use disorder (AUD) and anxiety disorders[38-40]. Women exhibit an accelerated onset of, and a higher probability for developing, AUD with the same history of alcohol use as their male counterparts in a phenomenon known as the telescoping effect[41]; and, binge-like patterns of alcohol consumption are increasingly prevalent, especially in women[42,43]. Both binge alcohol drinking and related diseases emerge in women during puberty when ovarian-derived E2 and related hormones begin to fluctuate across the menstrual cycle, and many have reported positive associations between circulating concentration of E2 and both alcohol drinking behavior and anxiolysis[44-49]. It has been broadly reported that female rodents consume more alcohol than their male counterparts[50-52]. Ovarian hormones contribute to this phenomenon, as removal of the ovaries reduces alcohol drinking and increases avoidance behavior[9,35,53], and chronic E2 administration in ovariectomized females can restore high alcohol drinking and anxiolysis in some cases[9,54-59]. Foundational work has established that E2 signaling promotes alcohol drinking in intact females, as knockdown or degradation of ERα attenuates alcohol consumption [35,60]. However, a specific mechanism for the role of endogenous, ovarian-derived E2 in intact female alcohol drinking and avoidance behavior has not been established.

Here, we show that both alcohol drinking and avoidance behavior in female mice dynamically fluctuate across the estrous cycle in accordance with systemic E2 levels, contributing to observed sex differences in these behaviors. We show that the pro-drinking, but not anxiolytic, effects of ovarian E2 occur via rapid nongenomic signaling at membrane-associated ERα in the bed nucleus of the stria terminalis (BNST), one of the most

sexually dimorphic brain regions that robustly expresses ERs[61,62]. Further, we find that BNST neurons that synthesize and release corticotropin releasing factor (CRF), a stress neuropeptide that has been highly linked to alcohol and anxiety-related behaviors[50,63-66] across mammalian species, are critical to the behavioral role of E2 via rapid E2-mediated increased excitatory synaptic transmission and enhancement of activity of $BNST^{CRF}$ neurons during motivated alcohol drinking behavior.

Results

Estrogen status across the estrous cycle dictates binge alcohol drinking and avoidance behavior

Prior studies have been unable to show dynamic modulation of alcohol drinking across the 4-5 day estrous cycle or a causal role for E2 in motivated alcohol drinking in gonadally intact female rodents, likely due to practical considerations including time of day of behavioral testing, potential disruption to estrous cyclicity by daily monitoring techniques, and the relatively transient peak of E2 during proestrus in rodents. Here, we validated and employed a minimally-invasive strategy to chronically monitor daily estrous cycle phase in intact female mice in close temporal proximity to behavioral testing during the dark phase of the light:dark cycle when mice are most active and consume the most alcohol (**Fig. 1a-d; Extended data Fig. 1a-c**). Two hours into the dark cycle each day, vaginal epithelial cells were collected via saline lavage and used to determine estrous cycle phase (**Fig. 1a**). Mice categorized as being in proestrus had higher ovarian expression of aromatase, the rate-limiting enzyme required for E2 synthesis (**Fig. 1b**), and higher blood plasma (**Fig. 1c**) and brain (**Fig. 1d**) E2 concentrations as measured by liquid chromatography tandem mass spectrometry (LC-MS/MS) than females in metestrus, confirming that mice categorized as being in proestrus using vaginal lavage-derived cytology were in a high ovarian E2 state (high E2) compared to those mice categorized as being in a low ovarian E2 state (low E2). Measures including estrous cycle length and the number of days in proestrus per estrous cycle were similar when lavage was performed in the light and dark phases of the light:dark cycle, and normal estrous cyclicity remained consistent across many weeks of daily monitoring (**Extended data Fig. 1a-c**). Therefore, we were able to use this vaginal cytology tracking strategy as an accurate, minimally-invasive proxy measure of real-time E2 status in intact female mice during behavioral testing in the dark phase without disrupting their natural estrous cyclicity and hormonal milieu.

We first employed this strategy to assess the effects of high E2 status during the estrous cycle on binge alcohol drinking using the standard drinking in the dark (DID) paradigm in which mice receive limited access (2-4 hours/day, 4 consecutive days per cycle) to 20% EtOH instead of their home cage water bottle (**Fig. 1e**). Across weekly cycles of EtOH DID, individual females consumed more alcohol when they were in a high E2 state in proestrus compared to when they were in other estrous cycle phases, with alcohol consumption during low E2 days increasing until it converged with the high E2 level by cycle six (**Fig. 1f**), demonstrating that individual females consume more alcohol when in a high ovarian E2 state than low ovarian E2 state. There was no significant difference in alcohol consumption between low E2 females and males, suggesting that ovarian E2 contributes to the higher consumption in females than males that we and others have previously reported[50,52,67]. Intriguingly, when females were specifically given their first access to alcohol in a high ovarian E2 state in proestrus, they consumed more alcohol than conspecifics given first access in a low E2 state (**Fig. 1g**), suggesting that prior experience with alcohol was not required for the pro-drinking effect of E2 status on binge drinking behavior. Further, there was no correlation between the cumulative number of alcohol drinking sessions in a high E2 state and alcohol consumption during subsequent low E2 sessions within individual mice across the six EtOH DID cycles (**Extended data Fig. 1d**), suggesting that the acute stimulatory effect of high E2 state on alcohol drinking was not directly related to the gradual escalation in low E2 alcohol consumption across DID cycles. In contrast to alcohol intake, estrous cycle did not affect consumption of 1% sucrose in a matched DID paradigm (sucrose DID; **Fig. 1h,i**). Females showed similar sucrose intake when in high and low E2 states and compared to males across cycles of sucrose DID (**Fig. 1h**) and during their first access to

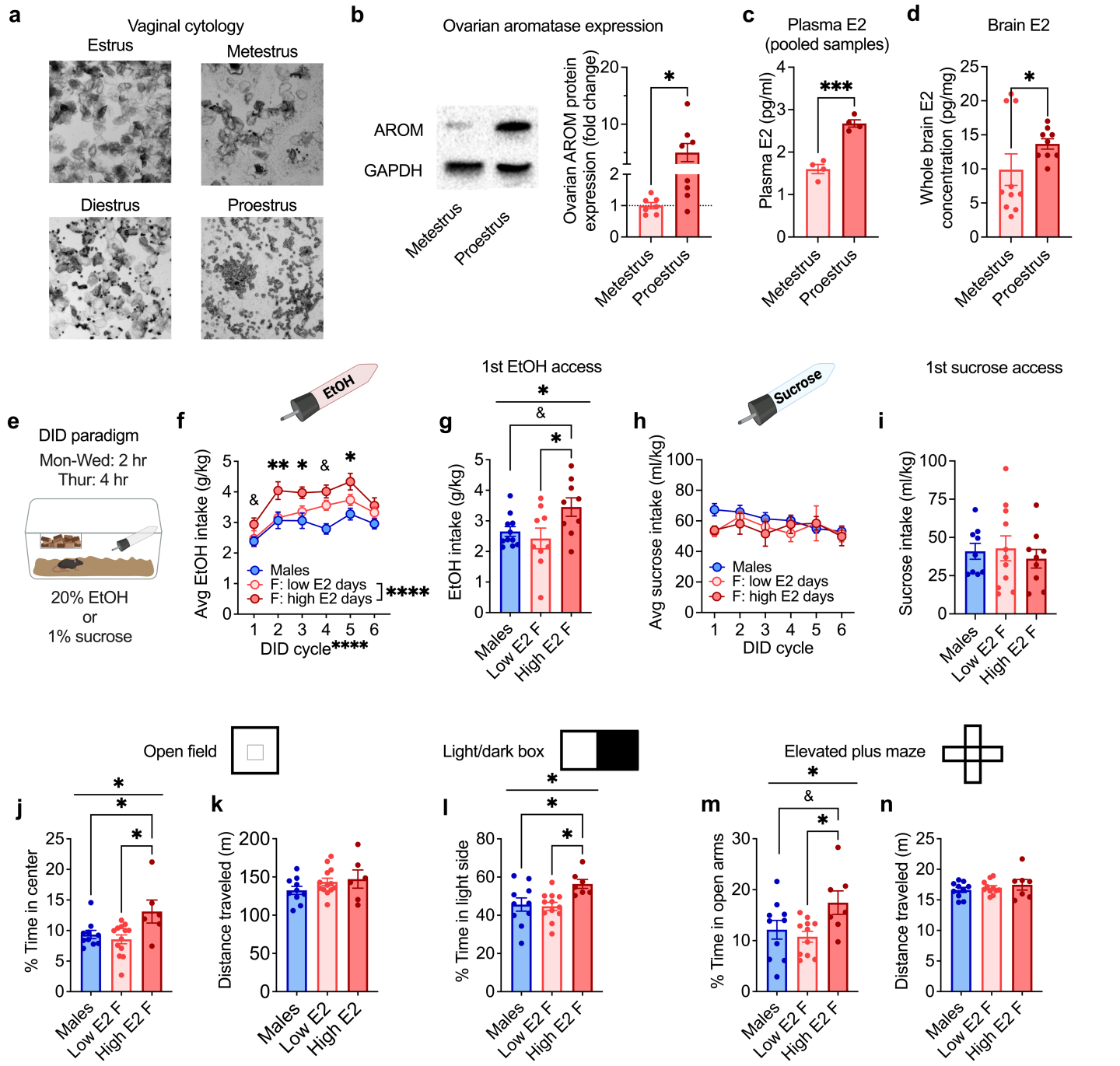

Figure 1: Binge alcohol drinking and avoidance behavior fluctuate with E2 status across the estrous cycle in gonadally-intact female mice. a-c) Minimally-invasive method for monitoring E2 status across the estrous cycle in gonadally-intact C57BL/6J mice. **a)** Representative images of vaginal epithelial cells in each estrous cycle phase in the female mouse. **b)** Aromatase (AROM) protein expression normalized to glyceraldehyde 3-phosphate dehydrogenase (GAPDH) was higher in the ovaries of female mice categorized by vaginal cytology as being in proestrus compared to mice categorized as being in metestrus. **c)** Plasma E2 concentrations were higher in proestrus compared to metestrus female mice, where each data point represents a pooled sample from five mice. **d)** Whole-brain E2 concentrations were higher in proestrus compared to metestrus mice. **e)** Schematic of the Drinking in the Dark (DID) binge consumption paradigm used in intact mice. **f)** High E2 status promoted average 2-hour consumption of 20% EtOH across cycles of EtOH DID. Within each DID cycle, individual females' average consumption on day(s) in proestrus when ovarian E2 was high vs. their days in other estrous cycle phases when ovarian E2 was low is included for each cycle in which mice had proestrus drinking day(s). **g)** Females given access to EtOH for the first time in a high E2 state (proestrus) displayed greater binge drinking than those given first access in a low E2 state and males. **h)** Estrous cycle did not modulate average 2-hour consumption of 1% sucrose across DID cycles (represented as in **e**). **i)** Females given access to sucrose

for the first time in a high E2 state displayed similar consumption as those given first access in a low E2 state and males. **j-n)** Females in a higher ovarian E2 state displayed reduced avoidance behavior compared to those in a low E2 state and males. **j)** % Time spent in the center of the open field test (OF) was higher in females in proestrus (high E2) than those in other estrous cycle stages (low E2) and males. **k)** There was no difference in distance traveled in the OF between high or low E2 status females or males. **l)** High E2 status female mice spent a greater % time on the light side of the light:dark box (LDB) than low E2 status females and males. **m)** High E2 status female mice spent a greater % time spent in open arms of the elevated plus maze (EPM) compared to low E2 status females and males. **n)** There was no difference in distance traveled in the EPM between high or low E2 status females or males. *P < 0.05, **P < 0.01, ***P < 0.001, ****P < 0.0001, $^{\&}$P < 0.10 for unpaired t-tests, mixed effects analysis main effects, one way ANOVA main effects of group, and post hoc t-tests paired t-tests with H-S corrections between high and low E2 days in **f** and post hoc unpaired t-tests with H-S corrections for other panels, as indicated. Detailed statistics are provided in **Supplemental Table 1**. Illustrations were created with biorender.com.

sucrose (**Fig. 1i**), suggesting the effects of ovarian E2 status on alcohol drinking are not generalized to palatable/rewarding substances or appetitive regulation.

High volume alcohol consumption is often associated with dysregulation of anxiety[68], and anxiety behavior itself is also sensitive to ovarian-derived E2 status in humans[46,49,69] and rodents[36,37,70]. To provide insight into whether ovarian E2 dynamically regulates avoidance behavior in intact female mice, we first performed a battery of avoidance behavior assays one week apart. Females in a high E2 state displayed an anxiolytic phenotype compared to conspecifics in a low E2 state and males, with greater percent time spent and distance in the center of the open field (OF), light side of the light:dark box (LDB), and open arms of the elevated plus maze (EPM), without any alteration in their overall locomotor behavior (**Fig. 1j-n; Extended data Fig. 1e,f**). Individual females' behavior varied across the battery according to their estrous cycle stage on each test day, suggesting that ovarian E2 is a critical real-time regulator of avoidance behavior at the individual level, even when mice have had prior experiences in experimentally-induced anxiogenic contexts.

High ovarian estrogen state enhances excitatory synaptic transmission in BNST^{CRF} neurons and their pro-alcohol drinking role

Data from human patients with alcohol use disorder and anxiety disorders show that the BNST is an important hub of neurocircuitry altered in these disease states[71], and the BNST is critical in the regulation of binge alcohol drinking and avoidance behavior in rodents[50,65]. While the BNST richly synthesizes and releases numerous neuropeptides, the stress neuropeptide CRF has been most robustly linked to alcohol consumption[72,73]. A major subpopulation of CRF expressing BNST neurons is critical for driving alcohol drinking in both sexes and avoidance behavior in males (females not examined)[50], and project to numerous regions associated with stress, reward, and alcohol use[74,75]. We recently reported that BNST^{CRF} neurons in females display greater basal excitability and glutamatergic synaptic transmission than in males, which may be related to their higher alcohol drinking, and that they are required for binge alcohol drinking in both sexes[50]. Here, using a multiplexed chemogenetic manipulation approach (**Extended data Fig. 2**), we replicated our previous finding that the activity of BNST^{CRF} neurons promote females' binge alcohol drinking (**Extended data Fig. 2c**), and we further found that it surprisingly does not modulate avoidance behavior in females (**Extended data Fig. 2d**) as we have previously found in males[50]. During slice electrophysiology recordings (**Fig. 2**), we found that BNST^{CRF} neurons from females in a high ovarian E2 state had a higher frequency, but not amplitude, of spontaneous excitatory postsynaptic currents (sEPSCs) than those from females in a low ovarian E2 state (**Fig. 2c,d**), leading to greater excitatory synaptic drive (a composite metric that takes into account both the frequency and amplitude of PSC events[50]; **Fig. 2e**). BNST^{CRF} neurons from high E2 females also displayed higher frequency, but not amplitude, of spontaneous inhibitory postsynaptic currents (sIPSCs; **Fig. 2g,h**), which was insufficient to enhance inhibitory synaptic drive (**Fig. 2i**). These results suggest that high ovarian-derived E2 may enhance the excitatory synaptic transmission onto BNST^{CRF} neurons, promoting alcohol drinking in females that contributes to their greater alcohol consumption than males.

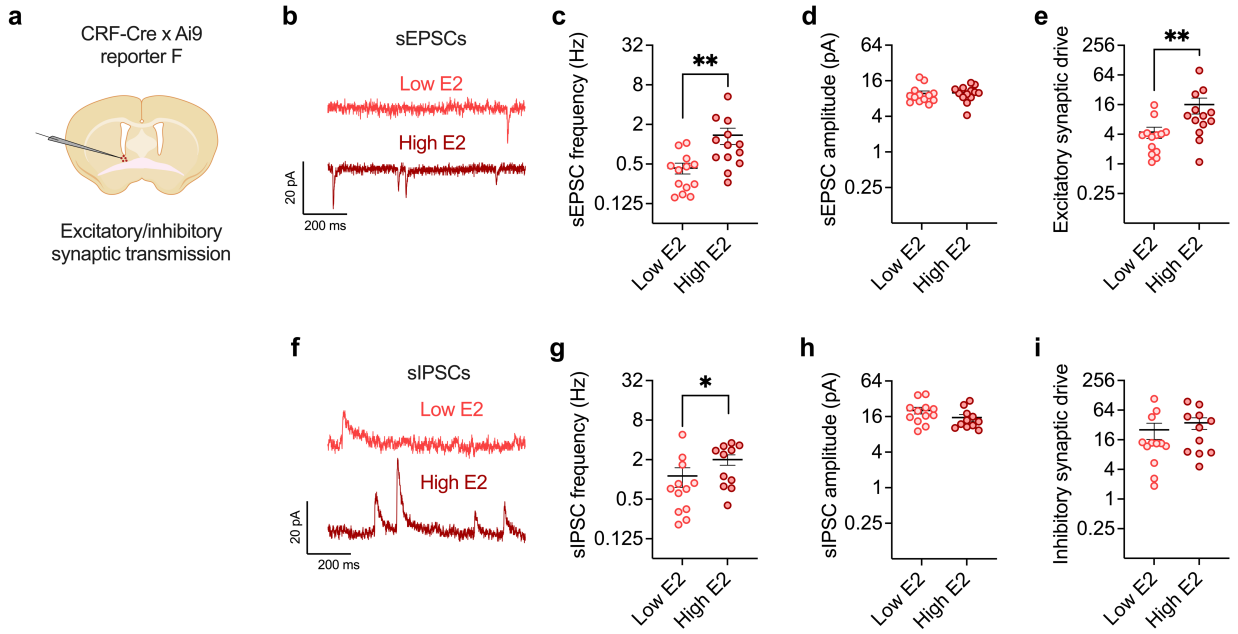

Fig. 2: BNST^{CRF} neurons are sensitive to ovarian estrogen status. a-i) Spontaneous synaptic transmission in BNST^{CRF} neurons as measured in slice electrophysiology recordings from intact CRF-CrexAi9 reporter females in low vs. high ovarian E2 states, with schematic in **a**. **b)** Representative traces of spontaneous excitatory postsynaptic currents (sEPSCs). **c)** The frequency of sEPSCs was higher in BNST^{CRF} neurons from high ovarian E2 females than those from low E2 females. **d)** sEPSC amplitude was unaffected by ovarian E2 status. **e)** The excitatory synaptic drive onto BNST^{CRF} neurons (frequency x amplitude) was greater in high vs. low ovarian E2 females. **f)** Representative traces of spontaneous inhibitory postsynaptic currents (sIPSCs). **g-i)** sIPSC frequency in BNST^{CRF} neurons was greater in high vs. low ovarian E2 status females (**g**), but amplitude (**h**) and synaptic drive (**i**) did not differ. *P < 0.05, **P < 0.01; unpaired t-tests between treatment groups and low E2 vs. high E2 groups. Detailed statistics are provided in **Supplemental Table 1**. Illustrations were created with biorender.com.

To examine whether ovarian E2 status regulates BNST^{CRF} neuron excitation *in vivo* during alcohol drinking behavior, we used the calcium biosensor GCaMP6s in BNST^{CRF} neurons as a proxy measure of population-level neuronal activity during a modified EtOH DID task. Mice received water access before (W1) and after (W2) the 20% EtOH access during each day of DID (**Fig. 3; Extended data Fig. 3**), and lickometer tracking of drinking behavior was used to characterize the temporal kinetics of and relationship between water/alcohol drinking, BNST^{CRF} neuron activity, and ovarian E2 status. We found that mice displayed greater motivated alcohol drinking, defined by more licking bouts (>1 s duration), when in a high E2 than low E2 state specifically during the first 30 minutes of EtOH access, including greater time spent drinking and higher average bout duration (**Fig. 3c,e,f;**). However, the total number of bouts, licking behavior, and fluid consumption across the entire access period did not differ between high E2 and low E2 drinking days (**Fig. 3d; Extended data Fig. 3d**). These data confirmed that the effects of ovarian E2 state on drinking within individual mice and across days of drinking were specific to alcohol rather than general fluid intake, and they point to the first 30 minutes of EtOH access as the most sensitive to E2 state-mediated regulation of alcohol drinking. Examination of BNST^{CRF} GCaMP activity during alcohol and water drinking showed that it ramped up at the onset of drinking bouts of EtOH, but not water, on both high E2 and low E2 drinking days (**Fig. 3h,i**), and the time spent drinking alcohol was positively correlated with average GCaMP signal during the first 30 minutes of EtOH access (**Fig. 3j**), suggesting that high BNST^{CRF} activation was associated with greater alcohol drinking.

Because females drank more alcohol early into access on high E2 days than low E2 days and consumption was correlated with BNST^{CRF} calcium activity, we posited that E2-dependent changes to GCaMP activity were related with behavioral changes in motivated drinking specifically across the transition between water and EtOH access. Indeed, we found that there was an increase in both the number of motivated drinking bouts and

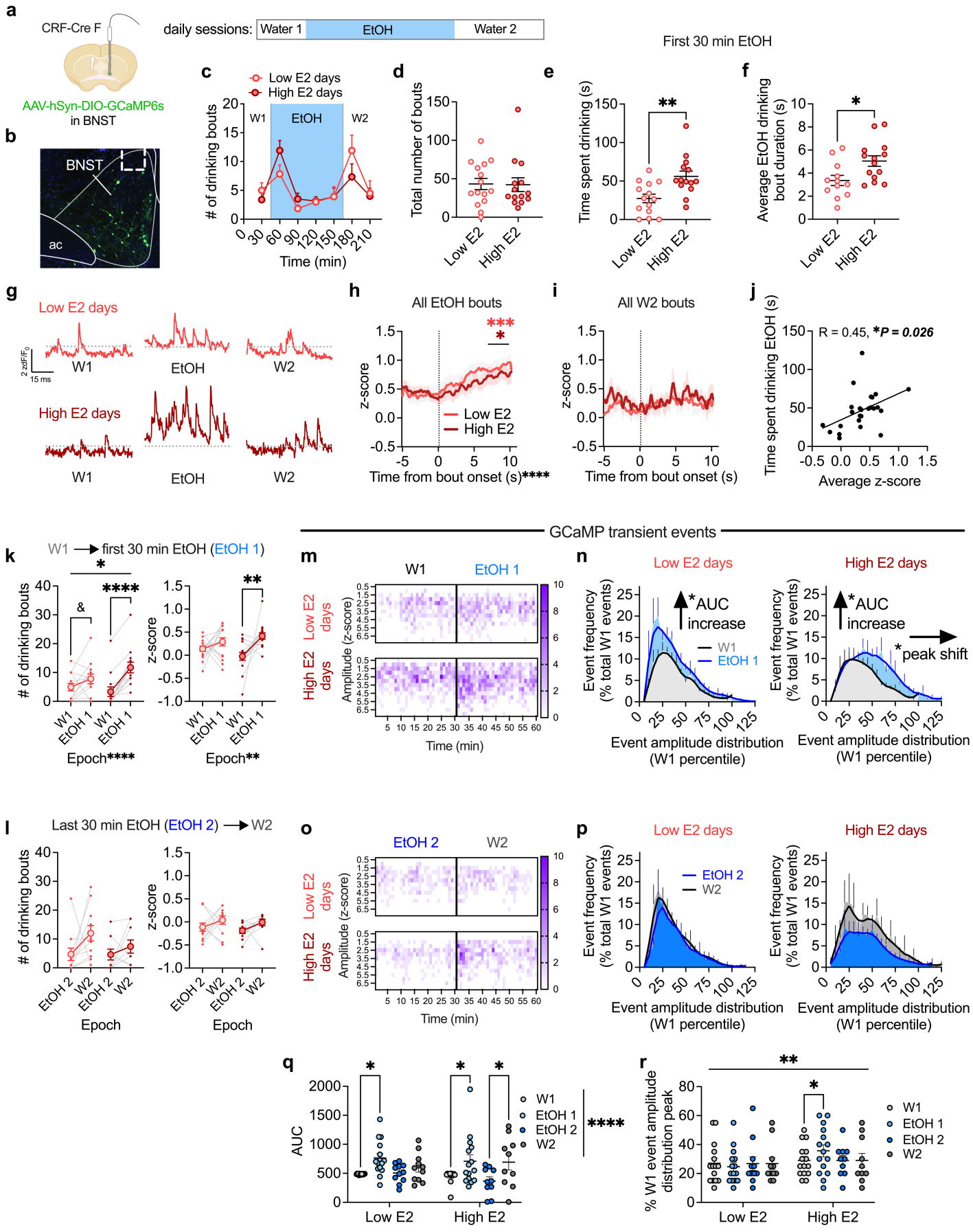
a
CRF-Cre F
AAV-hSyn-DIO-GCaMP6s
in BNST
daily sessions:
Water 1
EtOH
Water 2
First 30 min EtOH
b
BNST
ac
c
Low E2 days
High E2 days
W1
EtOH
W2
# of drinking bouts
Time (min)
d
Total number of bouts
Low E2
High E2
e
Time spent drinking (s)
f
Average EtOH drinking bout duration (s)
g
Low E2 days
High E2 days
W1
EtOH
W2
15 ms
h
All EtOH bouts
z-score
Low E2
High E2
Time from bout onset (s)****
i
All W2 bouts
Time from bout onset (s)
j
Time spent drinking EtOH (s)
R = 0.45, *P = 0.026
Average z-score
GCaMP transient events
k
W1 → first 30 min EtOH (EtOH 1)
# of drinking bouts
z-score
Epoch****
Epoch**
m
W1
EtOH 1
Low E2 days
High E2 days
Amplitude (z-score)
Time (min)
n
Low E2 days
High E2 days
Event frequency (% total W1 events)
*AUC increase
W1
EtOH 1
*peak shift
Event amplitude distribution (W1 percentile)
l
Last 30 min EtOH (EtOH 2) → W2
# of drinking bouts
z-score
EtOH 2
W2
Epoch
o
EtOH 2
W2
Low E2 days
High E2 days
Amplitude (z-score)
Time (min)
p
Low E2 days
High E2 days
Event frequency (% total W1 events)
EtOH 2
W2
Event amplitude distribution (W1 percentile)
q
AUC
W1
EtOH 1
EtOH 2
W2
****
Low E2
High E2
r
% W1 event amplitude distribution peak
W1
EtOH 1
EtOH 2
W2
Low E2
High E2

Fig. 3: Ovarian E2 state modulates the activity of BNST^{CRF} neurons during motivated alcohol drinking. Fiber photometry recordings of GCamP6s in BNST^{CRF} neurons during behavior, with schematic of unilateral viral injection and optical fiber cannula placement in **a** and representative image of GCaMP expression and fiber placement in **b**. **c)** Top: fiber photometry daily modified EtOH DID session timeline in which water access was given before (W1) and after (W2) the 2-hour EtOH access period. Bottom: time course showing drinking bouts across the water and EtOH epochs. **d)** The total number of drinking bouts across the entire session did not differ between high and low ovarian E2 status drinking days. **e-f)** Total time spent displaying motivated EtOH drinking (time in bout; **e**) and average EtOH drinking bout duration (**f**) were greater during the first 30 minutes of EtOH access on high E2 status drinking days than on low E2 status drinking days. **g)** Representative traces of GCaMP fiber photometry signal from one mouse on a low E2 drinking day (top) and high E2 drinking day (bottom), with signal z-scored to the entire drinking session for each day. **h-i)** GCaMP signal increased during both high and low E2 status drinking days across 10 s following bout onset for EtOH (**h**) but not water (**i**). **j)** There was a positive correlation between GCaMP signal and the time spent in motivated drinking during the first 30 minutes of EtOH access. **k)** The number of drinking bouts (left) and average GCaMP signal (right) increased during the first 30 minutes of EtOH access (EtOH 1) compared to W1 particularly during high E2 status drinking days. **l)** There was no change in bout number (left) or normalized GCaMP signal (right) in the first 30 minutes of W2 compared to the last 30 minutes of EtOH consumption (EtOH 2) on high E2 or low E2 status drinking days. **m)** Representative heat map of the frequency of GCaMP transient events across amplitude bins for a single mouse across W1 and EtOH 1 epochs on low (top) vs. high (bottom) E2 days. **n)** Frequency distribution of transient event amplitudes normalized to the amplitude distribution for W1 within each day during W1 and EtOH 1 epochs, showing that event number increased with the same amplitude distribution for low E2 drinking days (left) and with an increased amplitude distribution for high E2 drinking days (right). **o)** Representative heat map of the frequency of GCaMP transient events across amplitude bins across EtOH 2 and W2 epochs for the same mouse as in **l**. **p)** Frequency distribution of transient event amplitudes normalized to the amplitude distribution for W1 (left: low E2 days, right: high E2 days) during EtOH 2 and W2 epochs. **q**) Area under the curve (AUC) of GCaMP event distributions shown in **n** and **p** increased across W1→EtOH 1 epochs on both low E2 and high E2 drinking days and across EtOH 2→W2 epochs on high E2 drinking days. **r)** The peak of the event amplitude distributions shown in **n** and **p** was shifted rightward specifically during the EtOH 1 epoch on high E2 drinking days. *P < 0.05, **P < 0.01, ***P < 0.001, ****P < 0.0001, $^{\&}$P < 0.10 for unpaired t-tests, 2xANOVA main effects and interactions and their *post hoc* paired t-tests with H-S corrections, and Pearson's correlation as indicated. Detailed statistics are provided in **Supplemental Table 1**. Illustrations were created with biorender.com.

overall BNST^{CRF} neuron GCaMP activity across the W1 epoch and the first 30 minutes of EtOH (EtOH 1) on high E2 but not low E2 drinking days (**Fig. 3k**), while neither measure differed between the last 30 minutes of EtOH (EtOH 2) and second water (W2) epochs in either E2 state (**Fig. 3l**), again suggesting that E2 state-mediated changes in overall BNST^{CRF} neuron activity were related to alcohol drinking in particular. Analysis of the calcium transient events resulting from BNST^{CRF} neuron activity showed that the frequency of events increased across the W1→EtOH 1 epoch transition on both high E2 and low E2 days and across the EtOH 2→W2 epoch transitions on high E2 days, indicated by a greater area under the curve for the distribution of epoch event data normalized to W1 on each day (**Fig. 3m-q; Extended data Fig. 3e,h**). Further, specific examination of the temporal kinetics of event frequency, independent of amplitude, showed that it briefly (first 5 minutes) increased upon the presentation of a new bottle (containing either EtOH or water) regardless of E2 state (**Extended data Fig. 3f,i**), suggesting that BNST^{CRF} neuron activity is sensitive to the bottle cue and/or novelty associated with the bottle change, a known stimulator of consumption[76]. In contrast, event amplitude increased across the W1→EtOH 1 epoch transition, but not the EtOH 2→W2 epoch transition, and specifically on high E2 drinking days (**Fig. 3m-p,r; Extended data Fig. 3f,i**); this was indicated by a significant rightward shift for the frequency distribution of epoch event amplitude for the EtOH 1 epoch on high E2 drinking days (**Fig. 3m-p,r**), demonstrating that the added events during EtOH 1 specifically on high E2 days were larger in amplitude. This increase in event amplitude emerged at the onset of EtOH 1 and persisted throughout (**Fig. 3m; Extended data Fig. 3f,i**). Thus, in both high and low E2 states, the frequency of calcium transient events increased during alcohol consumption compared to W1, as indicated by an increase in AUC (**Fig. 3n,q**). However, the distributions show that in a low E2 state, these added events during EtOH 1 are of the same amplitude, while in a high E2 state the EtOH 1 added events have a greater amplitude compared to W1, indicated by the rightward shift in the amplitude distribution (**Fig. 3n,r**). These results suggest temporal summation of BNST^{CRF} neuron activity due to higher frequency action potential firing within the activated BNST^{CRF} population and/or greater coordinated activity across the population[77] during early alcohol access

when drinking in a high E2 state. As female BNST^{CRF} neurons project broadly across the extended amygdala, hypothalamus, thalamus, midbrain, and brainstem (**Extended Data Fig. 4**), a high E2 state may prime the increase in activity of specific BNST^{CRF} projection populations or recruitment of additional projections during alcohol access.

We also examined the E2 state-dependence of BNST^{CRF} neuron activity during avoidance behavior (**Extended data Fig. 3j,k**). Surprisingly, while BNST^{CRF} neuron GCaMP activity was sensitive to the anxiogenic context in both the EPM and OF assays, with highest activity in the open arms of the EPM and center of the OF and lowest activity in the closed arms of the EPM and corners of the OF, it did not differ between mice on high or low ovarian E2 status days. Altogether, these results suggest that high ovarian E2 state-dependent excitation of BNST^{CRF} neurons contributes to the pro-alcohol drinking, but not anxiolytic, phenotype observed in proestrus.

Rapid nongenomic E2 signaling in the BNST promotes binge alcohol drinking and increases excitatory synaptic transmission in BNST^{CRF} neurons

We next assessed the timescale on which ovarian E2 can regulate binge alcohol drinking and avoidance behaviors (**Fig. 4, Extended data Fig. 5**). We found that systemic administration of the aromatase inhibitor letrozole (LET) to acutely block E2 synthesis (and thus acutely reduce E2 bioavailability) dose-dependently suppressed binge alcohol consumption in females in a high ovarian E2 state (**Fig. 4a,b**) but not in a low ovarian E2 state (**Extended data Fig. 5a,b**). Acute LET administration had no effect on binge sucrose consumption in either high or low ovarian E2 females (**Extended data Fig. 5c**), suggesting that E2's role in promoting alcohol drinking is not due to modulation of general appetitive behavior or reward sensitivity.

In contrast to its effects on alcohol consumption, systemic administration of LET did not attenuate high E2-mediated anxiolysis in the EPM (**Fig. 4c; Extended data Fig. 5d**). And, acute intra-BNST infusion of LET did not alter binge alcohol consumption in high ovarian E2 status females (**Fig. 4d,e**), suggesting that the source of E2 synthesis driving the pro-binge drinking phenotype is not the BNST. Together, these results demonstrate that acute bioavailability and signaling of ovarian-derived E2 in the brain are necessary for the pro alcohol drinking, but not anxiolytic, effects of high ovarian E2 status. As E2 availability in real time was required for the pro-alcohol drinking effects of ovarian E2 status, we next sought to understand whether the BNST is a critical site for the behavioral effects of rapid E2 signaling, likely via nongenomic signaling at the cell membrane (**Fig. 4f-i**). We found that acute intra-BNST infusion of E2 (20 pg/side) in low E2 status females 10 minutes prior to behavioral testing rapidly enhanced binge alcohol consumption measured at one and two hours (**Fig. 4g**). We further found that intra-BNST infusion of a purified BSA-conjugated E2 that cannot cross the cell membrane and thus can only signal at the membrane (membrane-only E2, mE2), also rapidly increased binge alcohol drinking in low ovarian E2 status females at 1 hour (**Fig. h**). In contrast, acute intra-BNST infusion of E2 had no effect on avoidance behavior on the EPM (**Fig. 4i**). These results suggest that the BNST is a site for the rapid E2 signaling effects of high ovarian E2 status driving binge alcohol drinking behavior through nongenomic E2 signaling at membrane-associated ERs; further, they suggest that the E2-induced transcriptional program of high ovarian E2 status is not required for these pro-drinking effects but may be required for the anxiolytic effects of high ovarian E2 status.

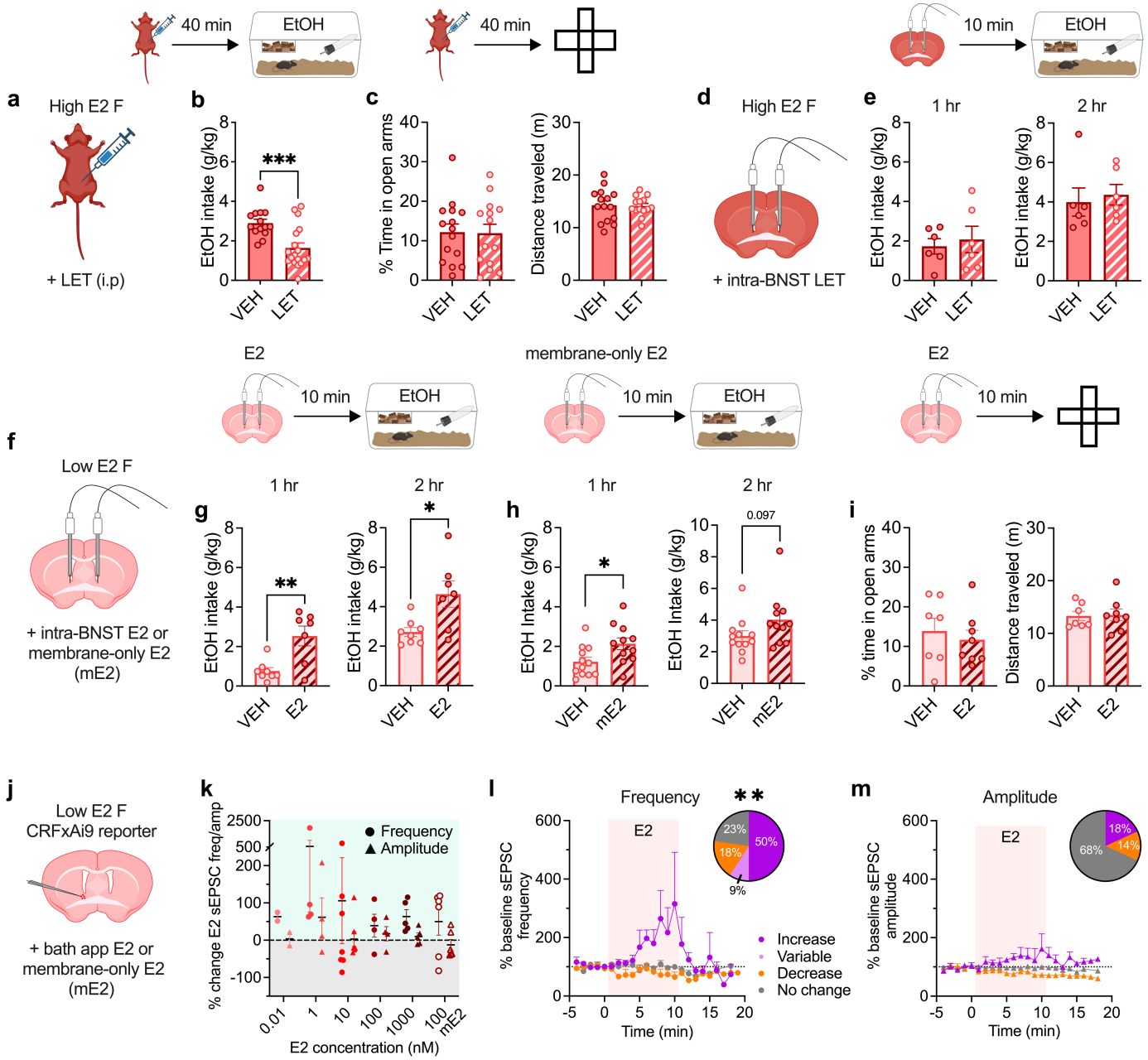

Figure 4: Rapid E2 signaling in the BNST recapitulates the pro-drinking but not anxiolytic effects of ovarian E2 and modulates BNST^{CRF} neurons. a-c) Effects of acute systemic E2 synthesis inhibition on behavior in high ovarian E2 status mice using systemic administration of the aromatase activity inhibitor letrozole (LET, 10 mg/kg, i.p.), as depicted in **a**. **b)** Acute LET administration 40 minutes prior to EtOH access suppressed binge EtOH consumption in high E2 status females. **c)** Acute LET administration in high E2 status females 40 minutes prior to the elevated plus maze (EPM) did not alter the % time spent in the open arms (left) or distance traveled (right). **d-e)** Effects of acute intra-BNST infusion of LET (1 µg in 200 nl/side) or saline vehicle controls (VEH) in high E2 status females on behavior, as depicted in **d**. **e)** Intra-BNST LET delivered 10 minutes prior to EtOH access did not alter binge EtOH consumption in high E2 status females at the 1-hour and 2-hour time points. **f-i)** Effects of acute intra-BNST infusion of E2 (20 pg in 200 nl/side) or BSA-conjugated, membrane-impermeable E2 (mE2, 55 pg in 200 nl/side) or saline vehicle controls (VEH) in low E2 status females on behavior, as depicted in **f**. **g)** Intra-BNST E2 delivered 10 minutes prior to EtOH access promoted binge EtOH consumption in low E2 status females at the 1-hour and 2-hour time points. **h)** Intra-BNST mE2, which cannot cross the cell membrane, delivered 10 minutes prior to EtOH access increased binge EtOH drinking in low E2 status females at the 1-hour timepoint with a trend at the 2-hour timepoint. **i)** Intra-BNST E2 delivered 10 minutes prior to testing on the EPM had no effect on % time spent in the open arms (left) or distance traveled (right). **j-m)** Effects of acute bath application of E2 and mE2 on excitatory synaptic transmission in BNST^{CRF} neurons during whole-cell slice electrophysiology recordings in low ovarian E2 status female CRF-CrexAi9 reporter mice, as depicted in **j**. **k)** Spontaneous excitatory postsynaptic currents (sEPSCs) maximum delta from % baseline during E2 (0.01-1000 nM) and mE2 (100 nM) wash on. **l)** Time course of BNST^{CRF} neurons that displayed an increase, decrease, or no change in sEPSC frequency % change from baseline

during the 10-minute application period and proportion of responding BNST^{CRF} neuron categories during E2 wash on (pie chart), showing a majority of low E2 status BNST^{CRF} neurons (50%) displayed increased frequency during E2 wash on. **m**) Time course of BNST^{CRF} neurons that displayed an increase, decrease, or no change in sEPSC amplitude % change from baseline during the 10-minute application period and responding BNST^{CRF} neuron categories during E2 wash on (pie chart), showing that the amplitude was unchanged in a majority of BNST^{CRF} neurons (68%). *P < 0.05, **P < 0.01, ***P < 0.001, unpaired t-tests between VEH vs. LET treatment and VEH vs E2/mE2 treatment; Fisher's exact test frequency vs amplitude; post hoc t-tests with H-S corrections as indicated. $^{\&}$P < 0.10 for t-tests. Detailed statistics are provided in **Supplemental Table 1**. Illustrations were created with biorender.com.

Because BNST^{CRF} neuron activation and acute E2 signaling in the BNST both rapidly enhanced binge alcohol drinking, we tested whether E2 rapidly promotes excitatory synaptic transmission in BNST^{CRF} neurons in slice electrophysiology recordings (**Fig. 4j-m**). We found that bath application of E2 across a range of doses (0.1 nM-1 μM) and mE2 (100 nM) robustly increased the frequency of sEPSCs in a large proportion of BNST^{CRF} neurons in low ovarian E2 females (**Fig. 4k,l; Extended data Fig. 6a,b**). sEPSC frequency was modulated by rapid E2signaling to a greater degree than sEPSC amplitude, and E2-mediated changes in sEPSC frequency and amplitude were independent of one another (**Fig. 4l,m; Extended data Fig. 6c,d**). The enhancement of sEPSC frequency by bath-applied E2 (**Fig. 4k,l**) recapitulated the effects observed in high E2 status females (**Fig. 2i,j**), peaking at an average of 355% of baseline during the 10 minute E2 application period and returning to baseline during washout (**Fig. 4l**). These data suggest that E2 signals via a rapid nongenomic mechanism to promote glutamatergic drive of a large subpopulation of BNST^{CRF} neurons, perhaps defined by projection population/circuit contribution (**Extended Data Fig. 4**), and this mechanism may contribute to the pro-alcohol drinking role of rapid E2 signaling in the BNST.

ERα mediates the effects of rapid E2 signaling in the BNST

To investigate the receptor(s) mediating E2 drive of alcohol drinking, we examined the expression of ERs in BNST circuits. Analysis of single nucleus RNA sequencing (snRNA-seq) dataset (GEO: GSE126836)[78] showed that ERα (*Esr1*) was robustly expressed in the BNST (29.3%), while ERβ (*Esr2*) was sparsely expressed (6.7%; **Fig. 5a-c**), and the membrane-only receptor GPER (*Gper1*) was nearly undetected (0.3%; not shown). ERα was enriched in subpopulations of BNST cells that modulate glutamatergic transmission at BNST^{CRF} synapses, including CRF neurons themselves, VGLUT2+ (*Slc17a6*) glutamatergic BNST neurons, and astrocytes (*Gfap)* that regulate synaptic glutamate levels (**Fig. 5a-c, Extended data Fig. 7a-d**). We confirmed ERα and ERβ expression profiles in the BNST using high-sensitivity RNAscope fluorescence *in situ* hybridization (FISH). ERα was robustly expressed and ERβ sparsely expressed in CRF+ neurons (**Fig. 5d**) and VGLUT2+ neurons (**Fig. 5e**) in the BNST. We then assessed whether ERα mediates rapid excitatory synaptic transmission in BNST^{CRF} neurons of high E2 females via bath application of the ERα antagonist methyl-piperidino-pyrazole (MPP; 3 μM; **Fig. 5f**). MPP rapidly reduced sEPSC frequency in the majority of cells (71.4%) by an average of 51.5% of baseline, with no significant effect on sEPSC amplitude (**Fig. 5g,h**, **Extended data Fig. 7e,f**). In contrast, MPP reduced sEPSC frequency in only 28.6% of low E2 status BNST^{CRF} neurons (**Extended data Fig. 7g-i**). This suggests that there is E2 tone in the BNST of high ovarian E2 females that contributes to greater sEPSC frequency via rapid signaling at ERα; the rapid nature of the effect of ERα antagonism points to E2-ERα signaling at the membrane mediating the effects of ovarian E2 modulation. Finally, we probed whether this rapid E2 signaling in the BNST of high E2 females was required for the behavioral effects of high ovarian E2 state using acute intra-BNST administration of the ERα antagonist MPP (10 μM), the ERβ antagonist 4-[2-phenyl-5,7-bis(trifluoromethyl)pyrazolo[1,5-a]pyrimidin-3-yl]phenol (PHTPP; 10 μM), or their control vehicles 10 minutes prior to behavioral testing (**Fig. 5i**). We found that acutely blocking ERα, but not ERβ, signaling in the BNST abolished the pro-alcohol drinking effects of high ovarian E2 status (**Fig. 5j**), with no effect of intra-BNST MPP in low ovarian E2 status females (**Extended data Fig. 7j,k**). Neither intra-BNST ERα nor ERβ antagonism affected avoidance behavior in high ovarian E2 status females (**Fig. 5k,l**). Altogether, our results suggest that rapid E2 signaling at membrane-bound ERα mediates the effects of E2 on BNST^{CRF} neuron excitation and is required for the pro-alcohol drinking effects of high ovarian

E2 status in intact female mice. In contrast, basal anxiety state that is sensitive to ovarian E2 status is unaffected by acute E2 manipulations; rather, the transcriptional program of high ovarian E2 status may be necessary for E2's anxiolytic effects.

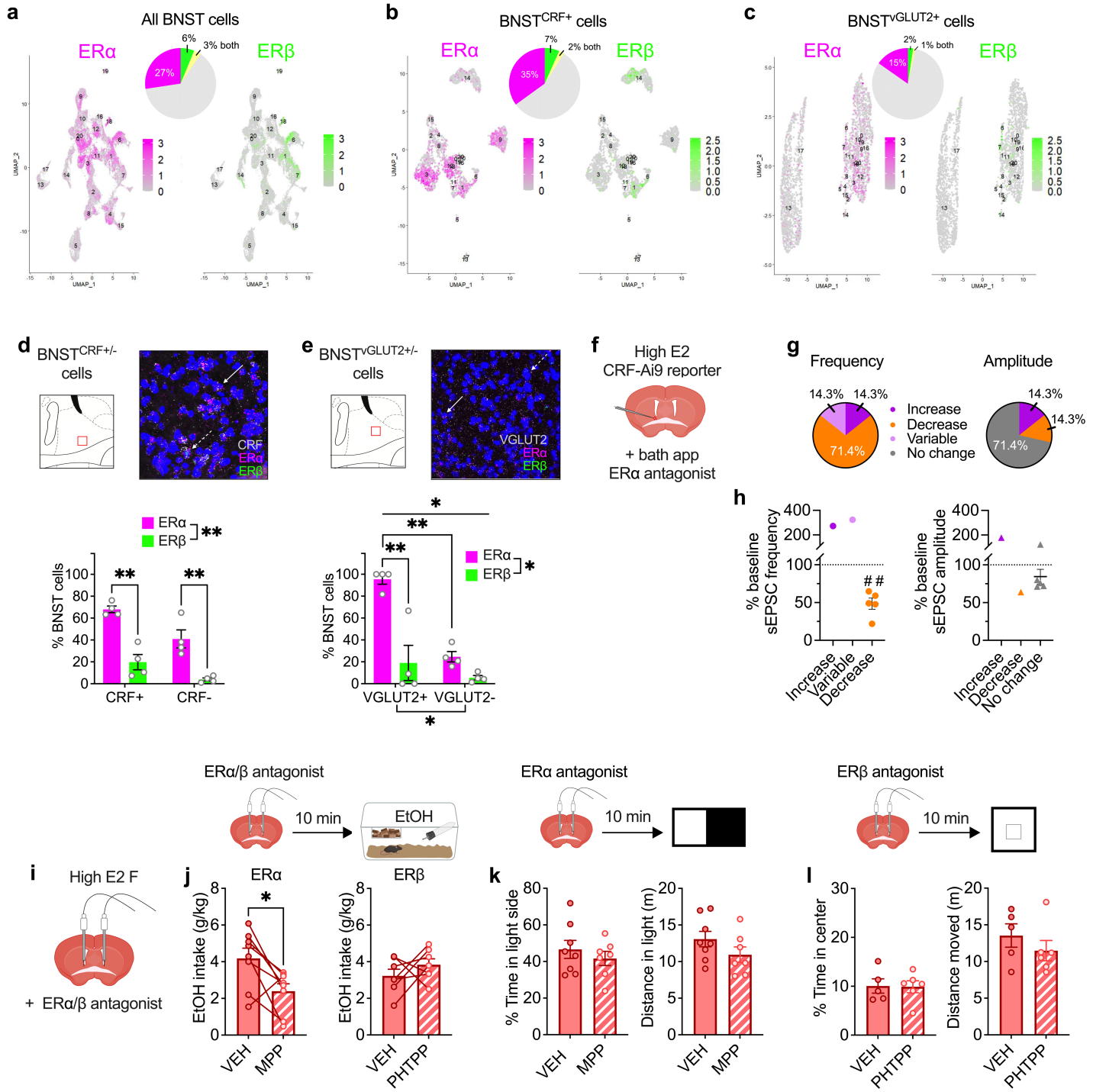

Figure 5: ERα is robustly expressed in the BNST and mediates rapid E2 modulation of binge drinking but not avoidance behavior. a-c) Analysis of single nucleus RNA sequencing (snRNA-seq) of female mouse BNST nuclei (total cells: 38,806; GEO: GSE126836)[78]. **a)** BNST cells expressing estrogen receptor α (ERα; *Esr1*, 27%) and estrogen receptor β (ERβ; *Esr2;* 6%) and both (3%). **b)** *Crh*-expressing BNST cells (BNST^{CRF}) expressing ERα (35%), ERβ (7%), and both (2%). **c)** *Slc17a6*-expressing BNST cells (BNST^{VGLUT2}) expressing ERα (15%), ERβ (2%), and both (1%). **d-e)** RNAscope fluorescence in situ hybridization (FISH) probing for ERα (*Esr1*), ERβ (*Esr2*), CRF (*Crh*), and VGLUT2 (*Slc17a6*) in the BNST in females, with red boxes within schematics (top left) indicating the location of confocal z-stack images taken and representative images pseudocolored for visibility (top right). **d)** ERα was expressed in more CRF+ cells than ERβ, with overall higher ERα expression in BNST CRF+ compared to CRF- cells. Solid arrow: cell expressing CRF/ERα/ERβ; dashed arrow: cell expressing CRF/ERα. **e)** ERα was expressed in more VGLUT2+ cells than ERβ, with

overall higher ERα expression in BNST VGLUT2+ compared to CRF- cells, showing a similar pattern to snRNA-seq expression. Solid arrow: cell expressing VGLUT2/ERα/ERβ; dashed arrow: cell expressing VGLUT2/ERα. **f-h)** Effects of acute bath application of the ERα antagonist methyl-piperidino-pyrazole (MPP) on excitatory synaptic transmission in $BNST^{CRF}$ neurons during whole-cell slice electrophysiology recordings in high ovarian E2 female CRF-CrexAi9 reporter mice, as depicted in **f**. Bath application of MPP (3 μM) reduced spontaneous excitatory postsynaptic current (sEPSC) frequency in a majority of cells during the 5 minute wash on period (**g**), while it had no effect on sEPSC amplitude (**h**). **i-l)** Effects of acute intra-BNST ERα or ERβ antagonism on behavior in high ovarian E2 status females. **i)** Depiction of strategy to site-deliver MPP (10 μM/200 nl/side), the ERβ antagonist 4-[2-phenyl-5,7-bis(trifluoromethyl)pyrazolo[1,5-a]pyrimidin-3-yl]phenol (PHTPP; 10 μM/200 nl/side), or saline vehicle (VEH) to the BNST in high E2 females via bilateral indwelling cannulae 10 minutes prior to behavioral testing. **j)** ERα antagonism via intra-BNST MPP reduced binge EtOH drinking in high ovarian E2 status females (left), with no effect of ERβ antagonism with PHTPP (right). **k)** ERα antagonism via intra-BNST MPP had no effect on avoidance behavior in the light:dark box (LDB). **l)** ERβ antagonism via intra-BNST PHTPP had no effect on avoidance behavior in the open field (OF). *P < 0.05, **P < 0.01, ***P < 0.001; 2xANOVA main effects and interactions between receptors; paired t-tests between VEH vs. ER antagonist treatment prior to DID; unpaired t-tests between VEH vs. ER antagonist treatment prior to avoidance assays; post hoc t-tests with H-S corrections as indicated. ## < 0.01; one sample t-test. Detailed statistics are provided in **Supplemental Table 1**. Illustrations were created with biorender.com.

Discussion

Here, we describe a critical role for rapid E2 signaling in driving binge drinking behavior in females. We found that estrous cycle status dictates behavioral phenotypes in female mice, as females displayed greater binge alcohol drinking and reduced avoidance behavior when they were in a high ovarian E2 state than when they were in a low ovarian E2 state (**Fig. 1**). However, the mechanisms driving these effects diverged, as rapid E2 signaling was required for the pro-alcohol drinking, but not anxiolytic, effects of high ovarian E2 (**Figs. 4 & 5**). Further, $BNST^{CRF}$ neuron activity was enhanced in a high E2 state during early alcohol access to promote motivated alcohol consumption, while it was neither necessary for nor sensitive to ovarian E2 state during avoidance behavior (**Figs. 2 & 3, Extended Data Fig. 3**). Intra-BNST E2 signaling, including that which could only signal at the cell membrane (mE2), rapidly promoted excitatory synaptic transmission in $BNST^{CRF}$ neurons and binge alcohol drinking in low E2 females (**Fig. 4**). And, ERα, which was densely and preferentially expressed within $BNST^{CRF}$ glutamatergic circuit components, mediated both the pro-drinking effects of high ovarian E2 state and its rapid enhancement of synaptic excitation of $BNST^{CRF}$ neurons (**Fig. 5**), as E2 increased these measures in low E2 mice and ERα antagonism reduced these measures in high E2, but not low E2, mice. Altogether, these results suggest that nongenomic E2 signaling at membrane-associated ERα in the BNST mediates the pro-drinking effects of ovarian E2 via excitation of $BNST^{CRF}$ neurons.

There is significant evidence of an association between E2 and alcohol consumption in humans[46,79], but the relationship between drinking and menstrual status has proven to be difficult to parse[80]. Careful monitoring of menstrual cycle stage and ovarian hormone status in nonhuman primates has been able to demonstrate that alcohol intake is modulated by fluctuating ovarian hormones across the menstrual cycle[81]. Previous work has shown that psychostimulant[32] and opioid-related[82] behaviors are modulated across the estrous cycle in rodents, however demonstrating estrous cycle modulation of alcohol drinking has proven to be challenging[9,51,83,84]. Nonetheless, many studies report that ovariectomy reduces alcohol intake[9,85] and E2 can enhance drinking in ovariectomized[9,56] and intact animals[57], suggesting a role for fluctuating E2 across the intact female rodent estrous cycle in alcohol drinking. Here, we validated a precise and accurate method for longitudinal monitoring of ovarian E2 status in intact female mice during behavior that allowed females to cycle normally. Using this, we provide the first evidence that fluctuating, rapidly acting ovarian-derived E2 is the source for the identified estrous cycle-dependent pro-drinking phenotype. In addition, we provide mechanistic insight into the role of ovarian E2 in alcohol drinking, showing that E2 signaling at membrane-associated ERα in the BNST drives binge alcohol drinking behavior. While intra-BNST membrane-only E2 (mE2) did increase alcohol consumption at the 1-hour timepoint, it should be noted that it did not have a robust effect at 2 hours, in contrast to intra-BNST free E2 (**Fig. 4**). This may suggest that while rapid E2 signaling via membrane bound ERs is critical for binge drinking, E2 may act through multiple mechanisms to regulate behavior. As males also

have robust expression of ERs in the BNST that mediate behavior[19], locally aromatized E2 in the BNST may be able to regulate binge alcohol drinking in males through a similar E2-dependent mechanism. This may be similar to what has been described for rapid E2 synthesis and signaling modulation of birdsong and reproduction in birdsong and hypothalamic nuclei in birds[27,30,86].

Here, we find that rapid signaling of ovarian E2 at membrane-associated receptors promotes excitatory synaptic transmission in $BNST^{CRF}$ neurons that drive motivated alcohol drinking. Although the link between rapid E2 signaling and acute behavioral control has not previously been described in gonadally-intact female rodents, there is a rich literature detailing signaling mechanisms of membrane-associated ER signaling in ex vivo and in vitro experiments[86-92]. This effect on synaptic excitation is similar to studies in the hippocampus and hypothalamus showing E2-mediated enhancement of glutamatergic mechanisms including glutamate release, dendritic spine formation, and long term potentiation[21,93-95]. The current reports on the role of rapid E2 in ovariectomized females on behavioral control show that social memory is dependent on rapid-E2 mediated ERK and PI3K actions in the hippocampus[22], and E2-mediated enhancement of cocaine self-administration requires mGluR5 activity[96], indicating the importance of excitatory synaptic transmission in E2's behavioral roles. Future work is necessary to fully elucidate the signaling mechanism underlying the role of rapid E2 in driving $BNST^{CRF}$ neuron activity to promote motivated alcohol drinking. Further, exogenous E2 and pharmacological activation of ERα rapidly increase alcohol-induced excitation of VTA dopamine neurons[60,97]. As the VTA is a primary target of $BNST^{CRF}$ neurons[75], and we found that a large subpopulation of $BNST^{CRF}$ neurons were sensitive to rapid E2 modulation, it is possible that E2 increases the activation of $BNST^{CRF}$ neurons that project to the VTA to directly synergize with E2 mechanisms there that promote dopamine release during alcohol drinking. Future work will be able to parse the specific $BNST^{CRF}$ and other neuronal populations sensitive to E2 modulation utilizing strategies including neural activity monitoring with single-cell resolution. However, future technical advancement in the miniaturization and stabilization of endoscopes is necessary to allow for long-term daily recording while maintaining normal estrous cyclicity and high levels of freely-moving voluntary binge drinking in female mice.

Intriguingly, while our data show that only rapid E2 signaling is needed for ovarian E2's role in alcohol drinking, they indicate that high ovarian E2-mediated anxiolysis instead may require E2-dependent transcriptional programming in the BNST and/or other brain regions. Consistent with another report[53], we found that acute modulation of E2 bioavailability did not alter avoidance behavior in intact females. And, there is ample evidence in the literature that ovariectomy increases avoidance behavior in female rodents[58,98]. However, the literature is mixed in the effects of E2 replacement, although only chronic administration has been evaluated[53,59,99]. Therefore, future work is needed to understand whether E2 is a critical mediator of estrous cycle modulation of avoidance behavior and to characterize the genomic effects by which it may act. Altogether, our results further our understanding of the mechanisms driving early alcohol drinking and states of anxiety in females, a critical step in understanding the role of a crucial neuromodulator and in developing effective interventions to minimize long-term negative health outcomes of alcohol drinking, especially in females.

Materials and Methods

Subjects
All experimental mice were male and female mice on a C57BL/6J background strain and ≥ 10 wks of age. Wildtype (WT) adult male and female C57BL/6J mice were purchased from Jackson Laboratory (Bar Harbor, ME, USA) at 8 weeks of age and all transgenic lines were bred in our animal facility. CRF-ires-Cre (CRF-Cre) [65] mice were bred with WT C57BL/6J mice, and hemizygous CRF-Cre mice were bred with homozygous floxed Ai9-tdTomato mice purchased from Jackson Laboratory to produce CRF-Cre-reporter mice. All mice were housed under a reverse circadian 12 h:12 h light:dark cycle with lights off at 7:30 am and *ad libitum* access to food and water. Mice were singly housed at least one week prior to behavioral testing and remained singly housed throughout the experimental procedures. Experiments began approximately 3 hours into the dark phase of the light:dark cycle. All procedures were conducted with approval of the Institutional Animal Care and Use Committee at Weill Cornell Medicine following the guidelines of the NIH Guide for the Care and Use of Laboratory Animals.

Estrous cycle monitoring
Estrous cycle stage was determined via daily lavage adapted from Mclean et al.[100], in which vaginal epithelial cells were collected with 15 µL 0.45% saline onto glass slides 1.5 hours into the dark cycle and analyzed for cell types corresponding to the different estrous cycle stages (depicted in **Fig. 1a**).

Tissue and plasma collection
Naïve female mice estrous cycles were tracked daily for at least two weeks. Following prolonged tracking, mice categorized via cytology as being in either the proestrus (high E2 ovarian status) or metestrus (low E2 ovarian status) stages were rapidly decapitated under isoflurane anesthesia. Whole blood was collected from the trunk into tubes precoated with K_2EDTA (BD Microtainer). The whole blood was immediately spun down in a standard centrifuge at 1,500 x g for 10 minutes at 4°C. The resulting plasma was collected and stored at -80°C until further analysis. Simultaneously, ovaries were dissected, frozen immediately on dry ice, and stored at -80°C.

Estrogen concentration measurement
Plasma
17β-Estradiol (E2) was quantified in pooled plasma samples by liquid chromatography-triple quadrupole tandem mass spectrometry (LC-MS/MS) using slight modifications of methods described previously[101]. Standard solutions of E2 (1.000 ± 0.005 mg/ml) and estradiol-2,4,16,16,17-d5 (E2-d5; 100 µg/ml) were obtained from Cerilliant (Round Rock, TX, USA) as 1 ml ampules with acetonitrile (ACN) as solvent. Charcoal-stripped human serum (CSS; Mass Spect Gold MSG3100, Golden West Biologicals, Temecula, CA, USA) was spiked with a working E2 standard stock (2 µg/ml) using a Hamilton syringe to yield a high calibration standard with a final E2 concentration of 4 ng/ml. Two-fold serial dilutions of the high calibration standard were prepared in CSS to yield 14 calibration standards including a blank (0 ng/ml). Three in-house serum pools (2 human, 1 nonhuman primate) were used as quality control (QC) samples. Calibration standards, QC samples, and pooled plasma samples (150 µl) were reverse-pipetted into 350 µl V-bottom 96-well microtiter plates (Shimadzu, Kyoto, Japan) followed by the addition of 100 µl of an internal standard spike (3.7 ng/ml E2-d5) into each well. Plates were shaken on an orbital shaker at room temperature for 1 hour and the contents of each well were transferred to 400 µl 96-well Isolute SLE+ plates (Biotage, Uppsala, Sweden) that had been washed with dichloromethane (DCM; 6 x 600 µl) and allowed to completely dry. Plates were equilibrated at room temperature for five minutes then eluted with DCM (3 x 600 µl) into 2 ml 96-well round bottom polypropylene plates (Analytical Sales & Services, Flanders, NJ, USA) containing 100 µl of 2-propanol per well. Plates were then subjected to positive pressure (~5 psi, 60 s) using a Pressure+ 96 positive pressure manifold (Biotage) to elute residual eluent. Eluates were evaporated to dryness under nitrogen at 40°C using a TurboVap 96 evaporation system (Biotage) and samples were reconstituted in 50 µL of 25:75 methanol:water (v/v) and transferred to new 350 µl V-bottom 96-well microtiter plates for analysis.

LC-MS/MS analysis was performed on a Shimadzu LCMS-8060 system. Twenty-five microliters of each reconstituted sample were injected from the microtiter plate (held at 10°C) onto a Raptor Biphenyl column (100 mm x 2.1 mm x 2.7 µm particle size; Restek, Bellefonte, PA, USA) with guard cartridge (5 mm x 2.1 mm x 2.7

µm particle size; Restek) held at 35°C. Analytes were eluted with an eluent gradient initially consisting of 35% mobile phase A (0.15 mM ammonium fluoride in water) and 65% mobile phase B (pure methanol) that was linearly changed to 97% B over 4 minutes and then to 100% B over 1.1 minutes. The column was then washed with 100% B for 1.8 minutes before being returned to 65% B over 0.1 minute and allowed to equilibrate for 3.4 minutes, for a total method time of 10.4 minutes. The flow rate was held constant at 0.4 ml/minute. Analytes were detected via heated electrospray ionization in negative ionization mode with scheduled multiple reaction monitoring (E2: 271.05 > 145.05 quantifier, > 143.05 reference; E2-d5: 276.20 > 187.10 quantifier, > 147.10 reference). Heating gas (air; 10 L/minute), drying gas (nitrogen; 10 L/minute), and nebulizing gas (nitrogen; 3 L/minute) were provided by a Peak Genius 1051 gas generator (Peak Scientific, Inchinnan, Scotland, UK). The interface temperature was 300°C, the heat block temperature was 400°C, and the desolvation line temperature was 250°C. Argon (Airgas) at 320 kPa was used as the collision gas. The source was equipped with a capillary B needle (Shimadzu) and capillary protrusion and probe distance were determined empirically based on maximizing E2 response. Shimadzu Lab Solutions software (version 5.97) was used to optimize the quadrupole pre-bias voltages and collision energies; the interface voltage -2 kV. The calibration curve was constructed using linear regression with 1/C weighting of the analyte/internal standard peak area ratio. The lower limit of quantification (LLOQ) for E2 was 1 pg/ml, defined as the lowest calibration curve concentration having an average accuracy of 80–120% and a CV of <20%[102].

Brain

Frozen brains (~450 mg) were sliced into ~50-75 mg sections and added to glass test tubes (12 x 75 mm) with 2 ml of cold (−20°C) acetonitrile and 50 µl of internal standard (14.8 ng/ml E2-d5 in 3:1 water:methanol, v:v). Samples were homogenized using a handheld homogenizer (Tissue Master 125, Omni International, Kennesaw, GA, USA) until a homogenous suspension formed. The homogenizer bit was then rinsed in 1 ml of acetonitrile in a separate tube and this solution was combined with the homogenate. The homogenizer was cleaned between samples by rinsing consecutively in methanol, 2-propanol, and water, followed by a final rinse in fresh methanol. Homogenates were stored at −20°C until further processing, at which point they were centrifuged and the supernatants transferred to new test tubes and dried under forced air at 37°C. Samples were resuspended in 200 µl of 3:1 water:methanol (v:v) and subjected to supported liquid extraction and analysis of E2 by LC-MS/MS as described for plasma samples except that the calibration standards (200 µl) were prepared in 3:1 water:methanol (v:v) and 50 µl of internal standard (14.8 ng/ml E2-d5 in 3:1 water:methanol, v:v) were used.

Western immunoblotting

Tissue was homogenized using a Teflon pestle (Pyrex, Illinois, USA) in cold RIPA buffer (Pierce, Massachusetts, USA) containing protease and phosphatase inhibitors. After spinning the homogenate at 12000 × g for 20 minutes, the supernatant was collected and used for western immunoblotting. Twenty µg of protein per sample were separated by 10% SDS-PAGE and transferred to polyvinylidene difluoride membranes, which were blocked in 5% nonfat dry milk and incubated 24-73 h at 4 °C in a primary antibody prior to being incubated in peroxidase-linked IgG conjugated secondary antibody at 1:5000 at room temperature for 1 h. Blots were incubated with aromatase (PA1-16532; Invitrogen, California, USA) diluted to 1:1000 and GAPDH (ab22555l; Abcam, Cambridge, UK) diluted to 1:40000. Proteins were quantified at the following molecular weights: aromatase at 55 kDa and GAPDH at 36 kDa. Protein bands were quantified as mean optical intensity using ImageJ software (NIH) and normalized to GAPDH. Normalized optical density values from each sample were used to calculate the fold change for each proestrus group compared with the metestrus group (set to 1.0) on the same blot.

Single nucleus RNA sequencing

Gene-expression matrices from female mouse BNST samples from dataset GEO: GSE126836[78] were loaded into R (v 4.3.1)[103] and preprocessed using Seurat[104]. We normalized the data using *NormalizeData.* Variable features were found using *FindVariableFeatures* using the vst selection method and nfeatures = 2000. Cells expressing genes of interest were subsetted and clustered. UMAPs showing co-expression of genes were generated with *FeaturePlot.*

RNAscope fluorescence in situ hybridization
Mice were euthanized under deep isoflurane anesthesia and their brains rapidly extracted, flash frozen in -35 °C 2-methylbutane, and stored at -80 °C under RNase-free conditions. Brains were embedded in OCT blocks with four brains per block, and 20 µM coronal sections were sliced on a cryostat and collected onto Superfrost Plus slides and stored at -80 °C in sealed slide boxes until undergoing *in situ* hybridization. Slides were thawed and in situ hybridization was conducted per manufacturer instructions using RNAscope Multiplex Fluorescent v1 kit with the HybEZ Oven and the following ACD probes: VGLUT2: mm-Slc17a6, cat #319171; CRF: mm-Crh, cat #316091; ERa: mm-Esr1, cat #478201; ERb: mm-Esr2, cat #316121. Slides were counterstained with DAPI and cover slipped with Vectashield. Images were acquired on a Zeiss LSM 880 Laser Scanning Confocal microscope in 1 µM plane z-stacks and manually analyzed in Metamorph according to RNAscope instructions to quantify the number of DAPI+ nuclei and number of DAPI+ cells expressing each probe alone or in combination. Representative images (**Fig. 4d,e**) were pseudocolored following analysis for color matching purposes using ImageJ (1.53a).

Drugs
Cyclodextrin-encapsulated E2 (Millipore Sigma, Massachusetts, USA) was dissolved in 0.9% saline, letrozole (LET; Tocris Bioscience, Bristol, UK) was dissolved in 5% dimethyl sulfoxide in 0.9% saline. MPP dichloride and PHTPP (Tocris Bioscience) were dissolved in 1% dimethyl sulfoxide and 0.9% saline. Membrane-only E2 (E2-BSA; Steraloids, Rhode Island, USA) was purified using Zeba™ Spin Desalting Columns, 7K (Thermo-Fischer, Massachusetts, USA) as follows: the column's storage solution was removed by centrifugal spinning at 1500 x g for 1 minute, then the column was conditioned with phosphate buffered saline (300 µl x 3). Membrane-only E2 (approx. 2 mg/minute in phosphate buffered saline, 120 µl) was loaded and eluted by centrifugal spinning at 1500 x g for 2 minutes. The exact concentration (36 µM) was assessed using BCA protein assay.

Stereotaxic surgery
For experiments requiring site-directed administration of viral vectors or cannulae implantation, mice were anesthetized with 2% isoflurane (VetEquip, CA, USA) in 0.8% oxygen in an induction chamber (VetEquip,) then placed in an Angle Two mouse stereotaxic frame (Leica Biosystems, Wetzlar, Germany) and secured with ear bars into a nose cone delivering isoflurane to maintain anesthesia. Mice were given a subcutaneous injection of meloxicam (2 mg/kg) for preemptive analgesia and 0.1 mL of 0.25% Marcaine around the incision site. For administration of viral vectors, a Neuros 7000 series 1 µL Hamilton syringe with a 33-gauge needle (Reno, NV) connected to a remote automated microinfusion pump (KD Scientific, Holliston, MA) was used for construct delivery at a rate of 50–100 nL/minute to the BNST (A/P: +0.3 mm, M/L: ±1.1 mm, D/V: −4.35 mm, 250 nL). Following infusion, the needle was left in place for 10 minutes and then slowly manually retracted to allow for diffusion and prevent backflow of the virus. Mice were continuously monitored for at least 30 minutes post-surgery to ensure recovery of normal breathing pattern and sternal recumbency and then checked daily. For cannulae implantation surgeries, bilateral cannulae (P Technologies, Virginia, USA) cut to 2.2 mm below the pedestal were secured with C & B Metabond dental cement at the same BNST coordinates used for viral infusions. The cannulae were secured with an internal dummy and plastic dust cap (P Technologies). For cannula histologies, mice were deeply anesthetized with isoflurane and 200 nL dye (Chicago Sky, Millipore Sigma) was infused. Brains were rapidly extracted from anesthetized animals and flash frozen, embedded in OTC, and sectioned at 45 µm on the cryostat to ensure placement of cannula. DREADD and fiber photometry brains were extracted, post-fixed overnight in 4% PFA, and then placed in PBS until they were sliced on the coronal plane in 45 µm sections on a VT1000S vibratome (Leica Biosystems, Wetzlar, Germany) to check injection placements and viral expression.

Behavior assays
<u>Drinking in the Dark</u>
The Drinking in the Dark (DID) binge alcohol drinking paradigm was used to model human binge consumption behavior in mice as previously described[50]. On Days 1-3 of each cycle of alcohol DID, three hours into the dark cycle, the home cage water bottle was replaced with a bottle containing 20% (v/v) ethanol for two hours and four hours on Day 4, followed by three days of abstinence between cycles. The same schedule was used to

evaluate binge sucrose consumption, except that home cage water bottles were replaced with 1% (w/v) sucrose. For all drinking experiments, empty "dummy" cages on the same rack as behavior mice received the same alcohol or sucrose bottle replacement, and consumption was adjusted for a leak from dummy bottles and then normalized to bodyweight.

Avoidance behavior

Avoidance behavior was assessed as previously described[52,65]. SMART software (Panlab, Barcelona, Spain) and Ethovision 15 (Noldus, Wageningen, Netherlands) video tracking were used to quantify raw locomotor and location data used to calculate measures including distance traveled and time spent. For basal avoidance behavior (**Fig. 1j-n**), assays were performed once per week within the same cohorts of mice.

Open field test

The open field test (OF) was conducted in a novel 50 × 50 cm plexiglass arena. Mice were placed in a corner of the arena, and time and distance in the center 50% of the apparatus vs. corners and periphery across the 30 minute trial were calculated.

Elevated plus maze

The elevated plus maze (EPM) was conducted in a plexiglass maze with two open and two closed arms (35 cm length × 5.5 cm width, with walls 15 cm tall in the closed arms). Mice were placed in the center of the EPM and time and distance in the open arms, closed arms, and center platform were calculated for the five minute trial.

Light:Dark Box

The light:dark box assay (LDB) was conducted in a rectangular box divided into two equal compartments (20 cm l × 40 cm w × 34.5 cm h) with one dark with a closed lid and the other with an open top and illuminated by two 60 W bulbs placed 30 cm above the box. The two compartments were separated by a divider with a 6 cm x 6 cm cut-out passageway at floor level. The mouse was placed in a corner of the light compartment and allowed to freely explore the apparatus, and the number of light side entries and time spent in the light vs. dark compartment were calculated for the 10 minute trial.

Pharmacological manipulations

Systemic LET (1 or 10 mg/kg[105,106]) or vehicle control were administered via intraperitoneal (i.p.) injection 40 minutes prior to alcohol or sucrose bottles being placed in the cages. For central infusions via cannulation, cyclodextrin-encapsulated E2 (20 pg), membrane-only E2 (55 pg), MPP (10 μM), or PHTPP (10 μM) in a total volume of 200 nL was infused bilaterally into BNST targeted guide cannulae using two Neuros 7000 series 1 μL Hamilton syringes with 33-gauge needles attached to a Harvard Apparatus pump. Ten minutes following BNST infusion, DID ethanol or sucrose bottles were placed into cages for DID or mice were placed in the testing apparatuses for avoidance assays.

Chemogenetic manipulations

CRF-Cre mice were injected with a cocktail of viral vectors containing Cre-dependent excitatory and inhibitory Designer Receptors Exclusively Activated only by Designer Drugs (DREADDs) (1:1 cocktail of the excitatory Gq-DREADD AAV2-hSyn-DIO-hM3D[Gq]-mCherry [125 nL] plus inhibitory Gi-KORD AAV8-hSyn-DIO-KORD[Gi]-mCitrine [125 nL]) or control virus (AAV2-hSyn-DIO-mCherry [250 nL]) in the BNST. After three weeks to allow for viral expression, mice underwent behavioral tests (conducted under 200-250 lux lighting conditions) to evaluate the role of the $BNST^{CRF}$ neurons in mediating avoidance behaviors and alcohol DID, All behavioral experiments/drinking sessions commenced three hours into the dark cycle, and each avoidance behavioral apparatus was thoroughly cleaned with 70% ethanol before each trial. For chemogenetic manipulation experiments, mice received vehicle (0.9% sterile saline, i.p.) or DREADD ligand dissolved in vehicle (CNO, 5 mg/kg, i.p., or SalB, 10-17 mg/kg, i.p.) injections 10-40 minutes prior to behavioral testing. Estrous cycle status was not monitored in DREADD behavioral experiments (EtOH DID, anxiety measures).

Fiber photometry

CRF-Cre mice expressing GCaMP6s in the BNST and a permanent fiber cannula implanted above the BNST were first habituated to handling and tethering of fiber optic patch cables during the week prior to the avoidance behavioral assays. Optical patch cables were photobleached through the fiber photometry

workstation (Tucker-Davis Technologies, Inc., Alachua, Florida) for at least 12 hours prior to being tethered to the mouse's head stage prior to each behavioral session. For drinking experiments, mice underwent a modified DID procedure in which they received water access prior to and after each 2-hour alcohol access. Drinking was measured using a capacitance based lickometer that elicited a TTL signal when licked, and a drinking bout was defined as at least 2 TTL pulses within one s, with a minimum bout length of 0.5 s. Raw fiber photometry signals (465 nm channel for GCaMP, 405 nm channel for the isosbestic point control) were collected at a sampling rate of 1017.25 Hz and denoised using a median filter to remove electrical artifacts and a lowpass filter to reduce high-frequency noise. To eliminate noise in the signal due to transfer to the behavioral apparatus or associated with bottle changes, the first 150 s for EPM, 400 s excluded for OF, and 1000 s for DID were excluded from analysis. The EPM trial length was increased to provide 5 minutes of analyzed data. The preprocessed data were down sampled by factor of 100 and corrected for photobleaching and motion artifacts by finding the best linear fit of the isosbestic control signal to the GCaMP signal and subtracting this estimated motion component from the GCaMP signal. Final z-score values were calculated by subtracting the mean of the whole trace from each datapoint and dividing it by the standard deviation of the trace. Data were analyzed based on behavioral epoch or tracked location. For EtOH DID, Fiber traces were segmented via a custom Python script from Jupyter open-source software to extract the last 30 minutes of W1, the first and last 30 minutes of EtOH, and the first 30 minutes of W2 as CSV files for each corresponding animal. Each file was converted into an Axon Binary File (integer)(*.abf) through the Clampfit 10.0 software. Peak analysis was executed in the Mini Analysis program Version 6. 0. 3 (Synaptosoft, USA). Detection parameters were adjusted per trace to automatically detect peaks that had a high ratio of signal to noise. Equal detection parameters were applied to each set of W1, EtOH, and W2 traces, grouped by the corresponding DID day. Each trace was manually checked by a blinded experimenter to eliminate false positives. Amplitude and frequency were binned and measured via Excel, and Graph Pad Prism 10.

Ex vivo slice electrophysiology

CRF-Cre reporter mice were rapidly decapitated under isoflurane anesthesia and their brains extracted. Brains were blocked on the coronal plane and acute 300 µm coronal slices prepared and incubated in carbogenated solutions with a pH of 7.35 and osmolarity of 305 as previously described [50]. Sections including BNST were sliced in N-methyl-D-glucamine (NMDG) artificial cerebrospinal fluid (NMDG-aCSF) at RT containing (in mM): 92 NMDG, 2.5 KCl, 1.25 NaH_2PO_4, 30 $NaHCO_3$, 20 HEPES, 25 glucose, 2 thiourea, 5 Na-ascorbate, 3 Na-pyruvate, 0.5 $CaCl_2 \cdot 2H_2O$, and 10 $MgSO_4 \cdot 7H_2O$. Slices were transferred to NMDG-aCSF at 32°C for 12-14 minutes, and then incubated for at least 1 hour at RT in HEPES-aCSF containing (in mM): 92 NaCl, 2.5 KCl, 1.25 NaH_2PO_4, 30 $NaHCO_3$, 20 HEPES, 25 glucose, 2 thiourea, 5 Na-ascorbate, 3 Na-pyruvate, 2 $CaCl_2 \cdot 2H_2O$, and 2 $MgSO_4 \cdot 7H_2O$. Slices were placed in the recording chamber and perfused at a rate of 2 ml/minute with 30°C normal aCSF containing (in mM): 124 NaCl, 2.5 KCl, 1.25 NaH_2PO_4, 24 $NaHCO_3$, 12.5 glucose, 5 HEPES, 2 $CaCl_2 \cdot 2H2O$, and 2 $MgSO_4 \cdot 7H_2O$, for at least 20 minutes prior to electrophysiological recordings. CRF+ (tdTomato-tagged) neurons were visualized using a 560 nm LED and 40× immersed objective with DsRed filter14. Basal synaptic transmission was measured in the voltage-clamp configuration using a cesium-methanesulfonate-based intracellular recording solution containing (in mM): 135 CsMeth, 10 KCl, 10 HEPES, 1 MgCl2·6H2O, 0.2 EGTA, 4 Mg-ATP, 0.3 Na2GTP, 20 phosphocreatine (pH 7.3, 290 mOsm) and driving force (−55 mV and +10 mV) to isolate excitatory and inhibitory transmission within individual neurons. The effects of E2 pharmacology on spontaneous excitatory postsynaptic currents (sEPSCs, 2 cells/mouse) were measured in a voltage clamp configuration using a cesium-gluconate-based intracellular recording solution containing (in mM): 117 D-gluconic acid, 20 HEPES, 0.4 EGTA, 5 TEA, 2 $MgCl_2$-$6H_2O$, 4 Na-ATP and 0.4 Na-GTP (pH 7.3 and 290 mOsm),) and a holding potential of -70 mV, using picrotoxin (25 µM) in the bath to block GABAergic synaptic transmission. E2 (1 nM, 10 nM, 100 nM, 1000 nM), mE2 (100 nM), or MPP (3 µM) in aCSF were washed on to measure their effects on excitatory synaptic transmission in separate experiments. Responder category threshold was defined as 15% delta of average drug wash on period OR 50% delta in a one minute period during drug wash on. Signals were acquired using a Multiclamp 700B amplifier (Molecular Devices), digitized, and analyzed via pClamp 10.4 or 11 software (Molecular Devices). Input resistance and access resistance were continuously monitored throughout experiments, and cells in which properties changed by more than 20% were not included in data analysis.

Statistical analyses

Statistical analyses were performed in GraphPad Prism 10. Data in each group for all dependent measures were checked for their distributions in raw and log space within the group and equality of variance across groups and analyzed accordingly. Statistical comparisons were always performed with an alpha level of 0.05 and using two-tailed analyses. Paired t-tests for within-subjects and unpaired t-tests for between-subjects direct comparisons were used to evaluate the effects of E2 modulators on alcohol drinking and avoidance behaviors. Two-way and three-way repeated measures ANOVAs (RM-ANOVAs) were used to examine the effects of cycle, groups, and drug and other repeated variables between mice in different experimental conditions; mixed effects models were used when one or more matched data point was unavailable. Following significant effects in ANOVAs, *post hoc* direct comparisons were performed using unpaired or paired t-tests with Holm-Sidak (H-S) correction for multiple comparisons, and adjusted p values are reported. Linear regressions were performed for correlation analyses. Data in figures are presented as mean ± SEM, and raw data points are included in all figures except some repeated measures graphs in which there were too many raw data points to be clearly represented. All statistics depicted in **Supplemental Table 1**.

References

1 Galea, L. A. M., Frick, K. M., Hampson, E., Sohrabji, F. & Choleris, E. Why estrogens matter for behavior and brain health. *Neurosci Biobehav Rev* **76**, 363-379 (2017). https://doi.org/10.1016/j.neubiorev.2016.03.024

2 Simpson, E. R. Sources of estrogen and their importance. *J Steroid Biochem Mol Biol* **86**, 225-230 (2003). https://doi.org/10.1016/s0960-0760(03)00360-1

3 Findlay, J. K., Liew, S. H., Simpson, E. R. & Korach, K. S. Estrogen signaling in the regulation of female reproductive functions. *Handb Exp Pharmacol*, 29-35 (2010). https://doi.org/10.1007/978-3-642-02062-9_2

4 Taxier, L. R., Gross, K. S. & Frick, K. M. Oestradiol as a neuromodulator of learning and memory. *Nat Rev Neurosci* **21**, 535-550 (2020). https://doi.org/10.1038/s41583-020-0362-7

5 Frick, K. M. & Kim, J. Mechanisms underlying the rapid effects of estradiol and progesterone on hippocampal memory consolidation in female rodents. *Horm Behav* **104**, 100-110 (2018). https://doi.org/10.1016/j.yhbeh.2018.04.013

6 Sharma, R., Cameron, A., Fang, Z., Ismail, N. & Smith, A. The regulatory roles of progesterone and estradiol on emotion processing in women. *Cogn Affect Behav Neurosci* **21**, 1026-1038 (2021). https://doi.org/10.3758/s13415-021-00908-7

7 Albert, K. M. & Newhouse, P. A. Estrogen, Stress, and Depression: Cognitive and Biological Interactions. *Annu Rev Clin Psychol* **15**, 399-423 (2019). https://doi.org/10.1146/annurev-clinpsy-050718-095557

8 Johnson, C. S. & Mermelstein, P. G. The interaction of membrane estradiol receptors and metabotropic glutamate receptors in adaptive and maladaptive estradiol-mediated motivated behaviors in females. *Int Rev Neurobiol* **168**, 33-91 (2023). https://doi.org/10.1016/bs.irn.2022.11.001

9 Satta, R., Hilderbrand, E. R. & Lasek, A. W. Ovarian Hormones Contribute to High Levels of Binge-Like Drinking by Female Mice. *Alcohol Clin Exp Res* **42**, 286-294 (2018). https://doi.org/10.1111/acer.13571

10 Kelly, M. J. & Rønnekleiv, O. K. Membrane-initiated estrogen signaling in hypothalamic neurons. *Mol Cell Endocrinol* **290**, 14-23 (2008). https://doi.org/10.1016/j.mce.2008.04.014

11 Tozzi, A., Bellingacci, L. & Pettorossi, V. E. Rapid Estrogenic and Androgenic Neurosteroids Effects in the Induction of Long-Term Synaptic Changes: Implication for Early Memory Formation. *Front Neurosci* **14**, 572511 (2020). https://doi.org/10.3389/fnins.2020.572511

12 Yoest, K. E., Quigley, J. A. & Becker, J. B. Rapid effects of ovarian hormones in dorsal striatum and nucleus accumbens. *Horm Behav* **104**, 119-129 (2018). https://doi.org/10.1016/j.yhbeh.2018.04.002

13 Evans, P. D. Rapid signalling responses via the G protein-coupled estrogen receptor, GPER, in a hippocampal cell line. *Steroids* **152**, 108487 (2019). https://doi.org/10.1016/j.steroids.2019.108487

14 Qiu, J., Rønnekleiv, O. K. & Kelly, M. J. Modulation of hypothalamic neuronal activity through a novel G-protein-coupled estrogen membrane receptor. *Steroids* **73**, 985-991 (2008). https://doi.org/10.1016/j.steroids.2007.11.008

15 Subbamanda, Y. D. & Bhargava, A. Intercommunication between Voltage-Gated Calcium Channels and Estrogen Receptor/Estrogen Signaling: Insights into Physiological and Pathological Conditions. *Cells* **11** (2022). https://doi.org/10.3390/cells11233850

16 Huang, G. Z. & Woolley, C. S. Estradiol acutely suppresses inhibition in the hippocampus through a sex-specific endocannabinoid and mGluR-dependent mechanism. *Neuron* **74**, 801-808 (2012). https://doi.org/10.1016/j.neuron.2012.03.035

17 Fernandez, S. M. *et al.* Estradiol-induced enhancement of object memory consolidation involves hippocampal extracellular signal-regulated kinase activation and membrane-bound estrogen receptors. *J Neurosci* **28**, 8660-8667 (2008). https://doi.org/10.1523/JNEUROSCI.1968-08.2008

18 Trainor, B. C., Lin, S., Finy, M. S., Rowland, M. R. & Nelson, R. J. Photoperiod reverses the effects of estrogens on male aggression via genomic and nongenomic pathways. *Proceedings of the National Academy of Sciences of the United States of America* **104**, 9840-9845 (2007). https://doi.org/10.1073/pnas.0701819104

19 Trainor, B. C., Finy, M. S. & Nelson, R. J. Rapid effects of estradiol on male aggression depend on photoperiod in reproductively non-responsive mice. *Hormones and behavior* **53**, 192-199 (2008). https://doi.org/10.1016/j.yhbeh.2007.09.016

20 Cross, E. & Roselli, C. E. 17beta-estradiol rapidly facilitates chemoinvestigation and mounting in castrated male rats. *Am J Physiol* **276**, R1346-1350 (1999). https://doi.org/10.1152/ajpregu.1999.276.5.R1346
21 Phan, A. *et al.* Rapid increases in immature synapses parallel estrogen-induced hippocampal learning enhancements. *Proc Natl Acad Sci U S A* **112**, 16018-16023 (2015). https://doi.org/10.1073/pnas.1522150112
22 Sheppard, P. A. S. *et al.* Social memory in female mice is rapidly modulated by 17β-estradiol through ERK and Akt modulation of synapse formation. *Proc Natl Acad Sci U S A* **120**, e2300191120 (2023). https://doi.org/10.1073/pnas.2300191120
23 Becker, J. B. Estrogen rapidly potentiates amphetamine-induced striatal dopamine release and rotational behavior during microdialysis. *Neurosci Lett* **118**, 169-171 (1990). https://doi.org/10.1016/0304-3940(90)90618-j
24 Hu, M. & Becker, J. B. Effects of sex and estrogen on behavioral sensitization to cocaine in rats. *J Neurosci* **23**, 693-699 (2003). https://doi.org/10.1523/JNEUROSCI.23-02-00693.2003
25 Hu, M., Crombag, H. S., Robinson, T. E. & Becker, J. B. Biological basis of sex differences in the propensity to self-administer cocaine. *Neuropsychopharmacology* **29**, 81-85 (2004). https://doi.org/10.1038/sj.npp.1300301
26 Cornil, C. A., Taziaux, M., Baillien, M., Ball, G. F. & Balthazart, J. Rapid effects of aromatase inhibition on male reproductive behaviors in Japanese quail. *Horm Behav* **49**, 45-67 (2006). https://doi.org/10.1016/j.yhbeh.2005.05.003
27 de Bournonville, M. P. *et al.* Rapid changes in brain estrogen concentration during male sexual behavior are site and stimulus specific. *Sci Rep* **11**, 20130 (2021). https://doi.org/10.1038/s41598-021-99497-1
28 Balthazart, J. *et al.* Rapid changes in production and behavioral action of estrogens. *Neuroscience* **138**, 783-791 (2006). https://doi.org/10.1016/j.neuroscience.2005.06.016
29 Remage-Healey, L., Coleman, M. J., Oyama, R. K. & Schlinger, B. A. Brain estrogens rapidly strengthen auditory encoding and guide song preference in a songbird. *Proc Natl Acad Sci U S A* **107**, 3852-3857 (2010). https://doi.org/10.1073/pnas.0906572107
30 Scarpa, G. B. *et al.* Estrogens rapidly shape synaptic and intrinsic properties to regulate the temporal precision of songbird auditory neurons. *Cereb Cortex* **33**, 3401-3420 (2023). https://doi.org/10.1093/cercor/bhac280
31 Taziaux, M., Keller, M., Bakker, J. & Balthazart, J. Sexual behavior activity tracks rapid changes in brain estrogen concentrations. *J Neurosci* **27**, 6563-6572 (2007). https://doi.org/10.1523/JNEUROSCI.1797-07.2007
32 Quigley, J. A., Logsdon, M. K., Graham, B. C., Beaudoin, K. G. & Becker, J. B. Activation of G protein-coupled estradiol receptor 1 in the dorsolateral striatum enhances motivation for cocaine and drug-induced reinstatement in female but not male rats. *Biol Sex Differ* **12**, 46 (2021). https://doi.org/10.1186/s13293-021-00389-w
33 Tonn Eisinger, K. R., Gross, K. S., Head, B. P. & Mermelstein, P. G. Interactions between estrogen receptors and metabotropic glutamate receptors and their impact on drug addiction in females. *Horm Behav* **104**, 130-137 (2018). https://doi.org/10.1016/j.yhbeh.2018.03.001
34 Torres Irizarry, V. C. *et al.* Estrogen signaling in the dorsal raphe regulates binge-like drinking in mice. *Transl Psychiatry* **14**, 122 (2024). https://doi.org/10.1038/s41398-024-02821-2
35 Chen, H. *et al.* Effect of a brain-penetrant selective estrogen receptor degrader (SERD) on binge drinking in female mice. *Alcohol Clin Exp Res* (2022). https://doi.org/10.1111/acer.14874
36 Hilderbrand, E. R. & Lasek, A. W. Estradiol enhances ethanol reward in female mice through activation of ERα and ERβ. *Horm Behav* **98**, 159-164 (2018). https://doi.org/10.1016/j.yhbeh.2018.01.001
37 Borrow, A. P. & Handa, R. J. Estrogen Receptors Modulation of Anxiety-Like Behavior. *Vitamins and hormones* **103**, 27-52 (2017). https://doi.org/10.1016/bs.vh.2016.08.004
38 Koob, G. F. Alcoholism: allostasis and beyond. *Alcoholism, clinical and experimental research* **27**, 232-243 (2003).
39 Grant, B. F. *et al.* Prevalence of 12-Month Alcohol Use, High-Risk Drinking, and DSM-IV Alcohol Use Disorder in the United States, 2001-2002 to 2012-2013: Results From the National Epidemiologic Survey on Alcohol and Related Conditions. *JAMA Psychiatry* **74**, 911-923 (2017). https://doi.org/10.1001/jamapsychiatry.2017.2161

40 Anker, J. J. & Kushner, M. G. Co-Occurring Alcohol Use Disorder and Anxiety: Bridging Psychiatric, Psychological, and Neurobiological Perspectives. *Alcohol Res* **40** (2019). https://doi.org/10.35946/arcr.v40.1.03
41 White, A. M. Gender Differences in the Epidemiology of Alcohol Use and Related Harms in the United States. *Alcohol Res* **40**, 01 (2020). https://doi.org/10.35946/arcr.v40.2.01
42 Vsevolozhskaya, O. A. & Anthony, J. C. Transitioning from First Drug Use to Dependence Onset: Illustration of a Multiparametric Approach for Comparative Epidemiology. *Neuropsychopharmacology* **41**, 869-876 (2016). https://doi.org/10.1038/npp.2015.213
43 Randall, C. L. *et al.* Telescoping of landmark events associated with drinking: a gender comparison. *J Stud Alcohol* **60**, 252-260 (1999). https://doi.org/10.15288/jsa.1999.60.252
44 Sarkola, T., Mäkisalo, H., Fukunaga, T. & Eriksson, C. J. Acute effect of alcohol on estradiol, estrone, progesterone, prolactin, cortisol, and luteinizing hormone in premenopausal women. *Alcohol Clin Exp Res* **23**, 976-982 (1999).
45 Muti, P. *et al.* Alcohol consumption and total estradiol in premenopausal women. *Cancer Epidemiol Biomarkers Prev* **7**, 189-193 (1998).
46 Martin, C. A., Mainous, A. G., Curry, T. & Martin, D. Alcohol use in adolescent females: correlates with estradiol and testosterone. *Am J Addict* **8**, 9-14 (1999). https://doi.org/10.1080/105504999306036
47 Strzelecki, A. M., Gipson, C. D., Childs, E. & Weafer, J. Preliminary evidence of increased alcohol use associated with ethinyl estradiol levels in women using oral contraceptives. *Drug Alcohol Depend Rep* **9**, 100194 (2023). https://doi.org/10.1016/j.dadr.2023.100194
48 Frydenberg, H. *et al.* Alcohol consumption, endogenous estrogen and mammographic density among premenopausal women. *Breast Cancer Res* **17**, 103 (2015). https://doi.org/10.1186/s13058-015-0620-1
49 Kundakovic, M. & Rocks, D. Sex hormone fluctuation and increased female risk for depression and anxiety disorders: From clinical evidence to molecular mechanisms. *Front Neuroendocrinol* **66**, 101010 (2022). https://doi.org/10.1016/j.yfrne.2022.101010
50 Levine, O. B. *et al.* The paraventricular thalamus provides a polysynaptic brake on limbic CRF neurons to sex-dependently blunt binge alcohol drinking and avoidance behavior in mice. *Nat Commun* **12**, 5080 (2021). https://doi.org/10.1038/s41467-021-25368-y
51 Priddy, B. M. *et al.* Sex, strain, and estrous cycle influences on alcohol drinking in rats. *Pharmacol Biochem Behav* **152**, 61-67 (2017). https://doi.org/10.1016/j.pbb.2016.08.001
52 Rivera-Irizarry, J. K. *et al.* Sex differences in binge alcohol drinking and the behavioral consequences of protracted abstinence in C57BL/6J mice. *Biol Sex Differ* **14**, 83 (2023). https://doi.org/10.1186/s13293-023-00565-0
53 Renczés, E. *et al.* The Role of Estrogen in Anxiety-Like Behavior and Memory of Middle-Aged Female Rats. *Front Endocrinol (Lausanne)* **11**, 570560 (2020). https://doi.org/10.3389/fendo.2020.570560
54 Ford, M. M., Eldridge, J. C. & Samson, H. H. Ethanol consumption in the female Long-Evans rat: a modulatory role of estradiol. *Alcohol* **26**, 103-113 (2002).
55 Ford, M. M., Eldridge, J. C. & Samson, H. H. Determination of an estradiol dose-response relationship in the modulation of ethanol intake. *Alcoholism-Clinical and Experimental Research* **28**, 20-28 (2004). https://doi.org/10.1097/01.Alc.0000108647.62718.5a
56 Rajasingh, J. *et al.* Enhanced voluntary alcohol consumption after estrogen supplementation negates estrogen-mediated vascular repair in ovariectomized mice. *Endocrinology* **148**, 3618-3624 (2007). https://doi.org/10.1210/en.2006-1357
57 Quirarte, G. L. *et al.* Estradiol valerate and alcohol intake: dose-response assessments. *BMC pharmacology* **7**, 3 (2007). https://doi.org/10.1186/1471-2210-7-3
58 Campos, G. V. *et al.* The Angiotensin Type 1 Receptor Antagonist Losartan Prevents Ovariectomy-Induced Cognitive Dysfunction and Anxiety-Like Behavior in Long Evans Rats. *Cell Mol Neurobiol* **40**, 407-420 (2020). https://doi.org/10.1007/s10571-019-00744-x
59 Fedotova, J., Pivina, S. & Sushko, A. Effects of Chronic Vitamin D_3 Hormone Administration on Anxiety-Like Behavior in Adult Female Rats after Long-Term Ovariectomy. *Nutrients* **9** (2017). https://doi.org/10.3390/nu9010028
60 Vandegrift, B. J. *et al.* Estrogen Receptor α Regulates Ethanol Excitation of Ventral Tegmental Area Neurons and Binge Drinking in Female Mice. *J Neurosci* **40**, 5196-5207 (2020). https://doi.org/10.1523/JNEUROSCI.2364-19.2020

61 Kelly, D. A., Varnum, M. M., Krentzel, A. A., Krug, S. & Forger, N. G. Differential control of sex differences in estrogen receptor α in the bed nucleus of the stria terminalis and anteroventral periventricular nucleus. *Endocrinology* **154**, 3836-3846 (2013). https://doi.org/10.1210/en.2013-1239
62 Weiser, M. J., Foradori, C. D. & Handa, R. J. Estrogen receptor beta in the brain: from form to function. *Brain Res Rev* **57**, 309-320 (2008). https://doi.org/10.1016/j.brainresrev.2007.05.013
63 Logrip, M. L., Koob, G. F. & Zorrilla, E. P. Role of corticotropin-releasing factor in drug addiction: potential for pharmacological intervention. *CNS Drugs* **25**, 271-287 (2011). https://doi.org/10.2165/11587790-000000000-00000
64 Rinker, J. A. *et al.* Extended Amygdala to Ventral Tegmental Area Corticotropin-Releasing Factor Circuit Controls Binge Ethanol Intake. *Biol Psychiatry* (2016). https://doi.org/10.1016/j.biopsych.2016.02.029
65 Pleil, K. E. *et al.* NPY signaling inhibits extended amygdala CRF neurons to suppress binge alcohol drinking. *Nat Neurosci* **18**, 545-552 (2015). https://doi.org/10.1038/nn.3972
66 Patel, R. R. *et al.* Synaptic effects of IL-1β and CRF in the central amygdala after protracted alcohol abstinence in male rhesus macaques. *Neuropsychopharmacology* **47**, 847-856 (2022). https://doi.org/10.1038/s41386-021-01231-y
67 Sneddon, E. A., Ramsey, O. R., Thomas, A. & Radke, A. K. Increased Responding for Alcohol and Resistance to Aversion in Female Mice. *Alcohol Clin Exp Res* **44**, 1400-1409 (2020). https://doi.org/10.1111/acer.14384
68 Guinle, M. I. B. & Sinha, R. The Role of Stress, Trauma, and Negative Affect in Alcohol Misuse and Alcohol Use Disorder in Women. *Alcohol Res* **40**, 05 (2020). https://doi.org/10.35946/arcr.v40.2.05
69 Handy, A. B., Greenfield, S. F., Yonkers, K. A. & Payne, L. A. Psychiatric Symptoms Across the Menstrual Cycle in Adult Women: A Comprehensive Review. *Harv Rev Psychiatry* **30**, 100-117 (2022). https://doi.org/10.1097/HRP.0000000000000329
70 Ryherd, G. L., Bunce, A. L., Edwards, H. A., Baumgartner, N. E. & Lucas, E. K. Sex differences in avoidance behavior and cued threat memory dynamics in mice: Interactions between estrous cycle and genetic background. *Horm Behav* **156**, 105439 (2023). https://doi.org/10.1016/j.yhbeh.2023.105439
71 Avery, S. N., Clauss, J. A. & Blackford, J. U. The Human BNST: Functional Role in Anxiety and Addiction. *Neuropsychopharmacology* **41**, 126-141 (2016). https://doi.org/10.1038/npp.2015.185
72 Kash, T. L. *et al.* Neuropeptide regulation of signaling and behavior in the BNST. *Mol Cells* **38**, 1-13 (2015). https://doi.org/10.14348/molcells.2015.2261
73 Schreiber, A. L. & Gilpin, N. W. Corticotropin-Releasing Factor (CRF) Neurocircuitry and Neuropharmacology in Alcohol Drinking. *Handb Exp Pharmacol* **248**, 435-471 (2018). https://doi.org/10.1007/164_2017_86
74 Dabrowska, J., Martinon, D., Moaddab, M. & Rainnie, D. G. Targeting Corticotropin-Releasing Factor Projections from the Oval Nucleus of the Bed Nucleus of the Stria Terminalis Using Cell-Type Specific Neuronal Tracing Studies in Mouse and Rat Brain. *J Neuroendocrinol* **28** (2016). https://doi.org/10.1111/jne.12442
75 Rinker, J. A. *et al.* Extended Amygdala to Ventral Tegmental Area Corticotropin-Releasing Factor Circuit Controls Binge Ethanol Intake. *Biol Psychiatry* **81**, 930-940 (2017). https://doi.org/10.1016/j.biopsych.2016.02.029
76 Wilcox, M. V. *et al.* Repeated binge-like ethanol drinking alters ethanol drinking patterns and depresses striatal GABAergic transmission. *Neuropsychopharmacology* **39**, 579-594 (2014). https://doi.org/10.1038/npp.2013.230
77 Mukai, Y., Nagayama, A., Itoi, K. & Yamanaka, A. Identification of substances which regulate activity of corticotropin-releasing factor-producing neurons in the paraventricular nucleus of the hypothalamus. *Sci Rep* **10**, 13639 (2020). https://doi.org/10.1038/s41598-020-70481-5
78 Welch, J. D. *et al.* Single-Cell Multi-omic Integration Compares and Contrasts Features of Brain Cell Identity. *Cell* **177**, 1873-1887.e1817 (2019). https://doi.org/10.1016/j.cell.2019.05.006
79 Hirko, K. A., Spiegelman, D., Willett, W. C., Hankinson, S. E. & Eliassen, A. H. Alcohol consumption in relation to plasma sex hormones, prolactin, and sex hormone-binding globulin in premenopausal women. *Cancer Epidemiol Biomarkers Prev* **23**, 2943-2953 (2014). https://doi.org/10.1158/1055-9965.EPI-14-0982

80 Carroll, H. A., Lustyk, M. K. & Larimer, M. E. The relationship between alcohol consumption and menstrual cycle: a review of the literature. *Arch Womens Ment Health* **18**, 773-781 (2015). https://doi.org/10.1007/s00737-015-0568-2
81 Dozier, B. L. *et al.* Chronic ethanol drinking increases during the luteal menstrual cycle phase in rhesus monkeys: implication of progesterone and related neurosteroids. *Psychopharmacology (Berl)* **236**, 1817-1828 (2019). https://doi.org/10.1007/s00213-019-5168-9
82 Smith, M. A. *et al.* Modulation of heroin intake by ovarian hormones in gonadectomized and intact female rats. *Psychopharmacology (Berl)* **238**, 969-978 (2021). https://doi.org/10.1007/s00213-020-05743-1
83 Radke, A. K., Sneddon, E. A., Frasier, R. M. & Hopf, F. W. Recent Perspectives on Sex Differences in Compulsion-Like and Binge Alcohol Drinking. *Int J Mol Sci* **22** (2021). https://doi.org/10.3390/ijms22073788
84 Finn, D. A. The Endocrine System and Alcohol Drinking in Females. *Alcohol Res* **40**, 02 (2020). https://doi.org/10.35946/arcr.v40.2.02
85 Sneddon, E. A., Masters, B. M., Shi, H. & Radke, A. K. Removal of the ovaries suppresses ethanol drinking and promotes aversion-resistance in C57BL/6J female mice. *Psychopharmacology (Berl)* **240**, 2607-2616 (2023). https://doi.org/10.1007/s00213-023-06456-x
86 Laredo, S. A., Villalon Landeros, R. & Trainor, B. C. Rapid effects of estrogens on behavior: environmental modulation and molecular mechanisms. *Front Neuroendocrinol* **35**, 447-458 (2014). https://doi.org/10.1016/j.yfrne.2014.03.005
87 Wnuk, A., Przepiórska, K., Pietrzak, B. A. & Kajta, M. Emerging Evidence on Membrane Estrogen Receptors as Novel Therapeutic Targets for Central Nervous System Pathologies. *Int J Mol Sci* **24** (2023). https://doi.org/10.3390/ijms24044043
88 Srivastava, D. P., Woolfrey, K. M. & Penzes, P. Insights into rapid modulation of neuroplasticity by brain estrogens. *Pharmacol Rev* **65**, 1318-1350 (2013). https://doi.org/10.1124/pr.111.005272
89 Srivastava, D. P. *et al.* Rapid estrogen signaling in the brain: implications for the fine-tuning of neuronal circuitry. *J Neurosci* **31**, 16056-16063 (2011). https://doi.org/10.1523/JNEUROSCI.4097-11.2011
90 Boulware, M. I. *et al.* Estradiol activates group I and II metabotropic glutamate receptor signaling, leading to opposing influences on cAMP response element-binding protein. *J Neurosci* **25**, 5066-5078 (2005). https://doi.org/10.1523/JNEUROSCI.1427-05.2005
91 Grove-Strawser, D., Boulware, M. I. & Mermelstein, P. G. Membrane estrogen receptors activate the metabotropic glutamate receptors mGluR5 and mGluR3 to bidirectionally regulate CREB phosphorylation in female rat striatal neurons. *Neuroscience* **170**, 1045-1055 (2010). https://doi.org/10.1016/j.neuroscience.2010.08.012
92 Qiu, J. *et al.* Rapid signaling of estrogen in hypothalamic neurons involves a novel G-protein-coupled estrogen receptor that activates protein kinase C. *J Neurosci* **23**, 9529-9540 (2003). https://doi.org/10.1523/JNEUROSCI.23-29-09529.2003
93 Jain, A. & Woolley, C. S. Mechanisms That Underlie Expression of Estradiol-Induced Excitatory Synaptic Potentiation in the Hippocampus Differ between Males and Females. *J Neurosci* **43**, 1298-1309 (2023). https://doi.org/10.1523/JNEUROSCI.2080-19.2023
94 Stincic, T. L., Grachev, P., Bosch, M. A., Rønnekleiv, O. K. & Kelly, M. J. Estradiol Drives the Anorexigenic Activity of Proopiomelanocortin Neurons in Female Mice. *eNeuro* **5** (2018). https://doi.org/10.1523/ENEURO.0103-18.2018
95 Smejkalova, T. & Woolley, C. S. Estradiol acutely potentiates hippocampal excitatory synaptic transmission through a presynaptic mechanism. *J Neurosci* **30**, 16137-16148 (2010). https://doi.org/10.1523/JNEUROSCI.4161-10.2010
96 Martinez, L. A. *et al.* Estradiol Facilitation of Cocaine Self-Administration in Female Rats Requires Activation of mGluR5. *eNeuro* **3** (2016). https://doi.org/10.1523/ENEURO.0140-16.2016
97 Vandegrift, B. J., You, C., Satta, R., Brodie, M. S. & Lasek, A. W. Estradiol increases the sensitivity of ventral tegmental area dopamine neurons to dopamine and ethanol. *PLoS One* **12**, e0187698 (2017). https://doi.org/10.1371/journal.pone.0187698
98 Arfa-Fatollahkhani, P. *et al.* The Effect of Luteinizing Hormone Reducing Agent on Anxiety and Novel Object Recognition Memory in Gonadectomized Rats. *Basic Clin Neurosci* **8**, 113-119 (2017). https://doi.org/10.18869/nirp.bcn.8.2.113

99 Miller, C. K. & Meitzen, J. No detectable changes in anxiety-related and locomotor behaviors in adult ovariectomized female rats exposed to estradiol, the ERβ agonist DPN or the ERα agonist PPT. *Horm Behav* **152**, 105363 (2023). https://doi.org/10.1016/j.yhbeh.2023.105363
100 McLean, A. C., Valenzuela, N., Fai, S. & Bennett, S. A. Performing vaginal lavage, crystal violet staining, and vaginal cytological evaluation for mouse estrous cycle staging identification. *J Vis Exp*, e4389 (2012). https://doi.org/10.3791/4389
101 Fecteau, K. M. *et al.* Comparison of assay methods for quantifying sex hormone concentrations across the menstrual cycle in rhesus macaques. *Biol Reprod* (2024). https://doi.org/10.1093/biolre/ioae063
102 Administration, U. S. F. a. D. (2018).
103 Team, R. C. (R Foundation for Statistical Computing, Vienna, Austria, 2021).
104 Hao, Y. *et al.* Integrated analysis of multimodal single-cell data. *Cell* **184**, 3573-3587.e3529 (2021). https://doi.org/10.1016/j.cell.2021.04.048
105 Inc., S. H. Letrozole Product Monograph. (2020).
106 Shah, M. Z. U. H. *et al.* Chlorogenic Acid Restores Ovarian Functions in Mice with Letrozole-Induced Polycystic Ovarian Syndrome Via Modulation of Adiponectin Receptor. *Biomedicines* **11** (2023). https://doi.org/10.3390/biomedicines11030900

Supplementary Materials

Supplemental Table 1 (statistics)

Extended data Figs. 1-7

Supplementary Table 1.

Figure	number of samples and exclusions	Statistical methods and values
1B	Met: N = 7; Pro: N = 9 (1 excl, irregular GAPDH band)	Unpaired t-test between metestrus and proestrus (t13 = 2.35, *P = 0.0349).
1C	Met: N = 20; Pro: N = 20; each sample is pooled from 5 mice	Unpaired t-test between metestrus and proestrus (t6 = 7.81, ***P = 0.0002).
1D	Met: N = 10; Pro: N = 9	All data log transformed (Y = ln[Y]); unpaired t-test between metestrus and proestrus status females (t17 = 2.24, **P = 0.0390).
1F	F: N = 27 (representing Pro and non-Pro matched data points within cycle for each mouse when Pro was captured); M: N = 7; across 6 wks of alcohol DID	Mixed effects analysis: Week (F5,176 = 9.97, ****P < 0.0001), Group (F2,58 = 11.09, ****P < 0.0001), interaction (F10,176 = 0.73, P = 0.6996). Post hoc paired t-tests with Holm-Sidak corrections between low E2 and high E2 status females for each week (1: t42 = 2.45, P = 0.0552; 2: t42 = 3.81, **P = 0.0027; 3: t42 = 3.10,*P = 0.0172; 4: t42 = 2.27, P = 0.0561; 5: t42 = 2.92, P = *0.0225; 6: t42 = 1.24, P = 0.2226). Post hoc unpaired t-tests with Holm-Sidak corrections between low E2 status females and males for each week (1: t135 = 0.02, P = 0.9903; 2: t135 = 0.12, P = 0.9903; 3: t135 = 0.63, P = 0.8948; 4: t135 = 2.27, P = 0.1409; 5: t135 = 1.43, P = 0.5664; 6: t135 = 0.99, P = 0.7882).
1G	M: N = 11; low E2 F: N = 10 (1 excl, bottle leak), high E2 F: N = 10 (1 excl, bottle leak)	One-way ANOVA: Group (F2,26 = 3.93,*P = 0.0323). Post hoc unpaired t-tests with Holm-Sidak corrections between: low E2 status females and males (t26= 0.62, P = 0.5414); high E2 status females and males (t26= 2.16, &P = 0.0782); low E2 status and high E2 status females (t26= 2.65, *P = 0.0398).
1H	F: N = 15 (representing Pro and non-Pro matched data points within cycle for each mouse when Pro was captured); M: N = 15; across 6 wks of sucrose DID	Mixed effects analysis: Week (F5,158 = 1.59, P = 0.1674), Group (F2,42 = 0.91, P = 0.4099), interaction (F10,158 = 0.96, P = 0.4822).
1I	Males: N = 10 (1 excl, erroneously high consumption based on distributions); low E2 status females: N = 11, high E2 status females: N = 10 (1 excl, erroneously high consumption based on distributions)	One-way ANOVA: Group (F2,26 = 0.26, P = 0.7755).
1J	Males: N = 10; low E2 status females: N = 13, high E2 status females: N = 6	One-way ANOVA: Group (F2,26 = 4.98, *P = 0.0147). Post hoc unpaired t-tests with Holm-Sidak corrections between: low E2 status females and males (t26= 0.63, P = 0.5339); high E2 status females and males (t26= 2.46, *P = 0.0417); low E2 status and high E2 status females (t26= 3.11, *P = 0.0135).
1K	Males: N = 10; low E2 status females: N = 13, high E2 status females: N = 6	One-way ANOVA: Group (F2,26 = 1.29, P = 0.2926).
1L	Males: N = 10; low E2 status females: N = 13, high E2 status females: N = 6	One-way ANOVA: Group (F2,26 = 4.71, *P = 0.0179). Post hoc unpaired t-tests with Holm-Sidak corrections between: low E2 status females and males (t26= 0.26, P = 0.7989); high E2 status females and males (t26= 2.57, *P = 0.0321); low E2 status and high E2 status females (t26= 2.90, *P = 0.0225).

1M	Males: N = 10; low E2 status females: N = 12 (1 excl, freezing in open arms), high E2 status females: N = 7	One-way ANOVA: Group (F2,25 = 3.88, *P = 0.0340). Post hoc unpaired t-tests with Holm-Sidak corrections between: low E2 status females and males (t25 = 0.62, P = 0.5423); high E2 status females and males (t25 = 2.12, &P = 0.0863); low E2 status and high E2 status females (t25 = 2.72, *P = 0.0348).
1N	Males: N = 10; low E2 status females: N = 12 (1 excl, freezing in open arms), high E2 status females: N = 7	One-way ANOVA: Group (F2,25 = 0.62, P = 0.5450).
s1A	Dark: N = 15; light: N = 21	Unpaired t-test between dark and light cycle females (t34 = 1.00, P = 0.3250).
s1D	Females: N = 27 (DID cycles 1-2: 8 excluded for zero days in proestrus or zero low E2 consumption; DID cycles 3-4: 6 excluded for zero low E2 consumption; DID cycles 5-6: 1 excluded for zero low E2 consumption	Simple linear regression: DID cycles 1-2: R = 0.248, P = 0.3062; DID cycles 3-4: R = 0.245, P = 0.2838; DID cycles 5-6: R = 0.247, P = 0.2241.
s1E	Males: N = 10; low E2 F: N = 13, high E2 F: N = 6	One-way ANOVA: Group (F2,26 = 8.07, **P = 0.0019). Post hoc unpaired t-tests with Holm-Sidak corrections between: low E2 status females and males (t26= 0.73, P = 0.4693); high E2 status females and males (t26= 3.17, **P = 0.0078); low E2 status and high E2 status females (t26= 3.94, P = 0.0016).
s1F	Males: N = 10; low E2 F: N = 12 (1 excl, freezing in open arms), high E2 F: N = 7	One-way ANOVA: Group (F2,25 = 4.71, *P = 0.0184). Post hoc unpaired t-tests with Holm-Sidak corrections between: low E2 status females and males (t25 = 1.30, P = 0.2050); high E2 status females and males (t25 = 1.86, P = 0.1447); low E2 status and high E2 status females (t25 = 3.07, *P = 0.0153).
2C	Low E2: N = 6, n = 16 cells (3 excl, noise); high E2: N = 7, n = 17 cells (4 excl, noise)	All data log transformed (Y = ln[Y]); unpaired t-test between low E2 and high E2 status females (t24 = 3.44, **P = 0.0021).
2D	Low E2: N = 6, n = 16 cells (3 excl, noise); high E2: N = 7, n = 17 cells (4 excl, noise)	All data log transformed (Y = ln[Y]); unpaired t-test between low E2 and high E2 status females (t24 = 0.29, P = 0.7748).
2E	Low E2: N = 6, n = 16 cells (3 excl, noise); high E2: N = 7, n = 17 cells (4 excl, noise)	All data log transformed (Y = ln[Y]); unpaired t-test between low E2 and high E2 status females (t24 = 2.83, **P = 0.0092).
2G	Low E2: N = 6, n = 14 cells (2 excl, noise); high E2: N = 7, n = 14 cells (3 excl, noise)	All data log transformed (Y = ln[Y]); unpaired t-test between low E2 and high E2 status females (t21 = 2.20, *P = 0.0395).
2H	Low E2: N = 6, n = 14 cells (2 excl, noise); high E2: N = 7, n = 14 cells (3 excl, noise)	All data log transformed (Y = ln[Y]); unpaired t-test between low E2 and high E2 status females (t21 = 1.52, P = 0.1427).
2I	Low E2: N = 6, n = 14 cells (2 excl, noise); high E2: N = 7, n = 14 cells (3 excl, noise)	All data log transformed (Y = ln[Y]); unpaired t-test between low E2 and high E2 status females (t21 = 1.12, P = 0.2740).
s2C	CON: N = 7, KORD: N = 7 (2 excl, misses)	2xRM-ANOVA: DREADD (F1,10 = 0.09, P = 0.7667), SalB (F1,10 = 5.24, *P = 0.0450), interaction (F1,10 = 4.41, P = 0.0620). Post hoc paired t-tests with Holm-Sidak corrections between VEH and SalB within group (CON: t10 = 0.15, P = 0.8864; KORD: t10 = 2.87, *P = 0.0328).
s2D	CON: N = 7 (1 excl, freezing in open arms), KORD: N = 7 (2 excl, misses)	Percent time in open arms: unpaired t-test between CON and KORD (t13 = 0.06, P = 0.9502); distance traveled: unpaired t-test between CON and KORD (t13 = 1.33, P = 0.2074).
s2F	CON: N = 8 (1 excl, VEH drinking < 1 g/kg), DREADD: N = 9 (3 excl: 2 misses, 1 VEH drinking < 1 g/kg)	2xRM-ANOVA: DREADD (F1,10 = 0.16, P = 0.7018), CNO (F1,10 = 0.81, P = 0.3895), interaction (F1,10 = 0.19, P = 0.6707).

s2G	CON: N = 14, DREADD: N = 14 (5 excl, misses)	Percent time in center: unpaired t-test between CON and DREADD (t21 = 0.14, P = 0.8893); distance traveled: unpaired t-test between CON and DREADD (t21 = 2.67, *P = 0.0142).
3D	N = 5, low E2 days = 15, high E2 status days = 15 (1 excl, technical error)	Unpaired t-test between low E2 status and high E2 status females (t27 = 0.079, P = 0.9373).
3E	N = 5, low E2 days = 15 (1 excl, technical error), high E2 status days = 15 (1 excl, technical error)	Unpaired t-test between low E2 status and high E2 status females (t26 = 3.24, **P = 0.0033).
3F	N = 5, low E2 days = 15 (3 excl: 1 technical error, 2 w/ 0 bouts), high E2 days = 15 (1 excl, technical error)	Unpaired t-test between low E2 status and high E2 status females (t24 = 2.61, *P = 0.0153).
3H	N = 5, low E2 days = 15 (2 excl, trace technical error), high E2 days = 15	2xRM-ANOVA: Time (F2,52 = 13.58, ****P < 0.0001), Estrous (F1,26 = 0.28, P = 0.5993), interaction (F2,52 = 1.12, P = 0.3339). Post hoc paired t-tests with Holm-Sidak corrections between 5 s bins (1: 5 s prior to bout onset, 2: 0-5 s after bout onset, 3: 6-10 s after bout onset; 15 s total) within group: low E2 status (bin 1 vs bin 2: t52 = 1.94, P = 0.1115; bin 1 vs bin 3: t52 = 4.42, ***P = 0.0003; bin 2 vs bin 3: t52 = 2.48, P = 0.0639); high E2 status (bin 1 vs bin 2: t52 = 0.32, P = 0.7493; bin 1 vs bin 3: t52 = 2.74, *P = 0.0416; bin 2 vs bin 3: t52 = 2.42, P = 0.0639).
3I	N = 5, low E2 days = 15 (2 exc, trace technical error), high E2 days = 15	2xRM-ANOVA: Time (F2,38 = 1.63, P = 0.2097), Estrous (F1,19 = 0.29, P = 0.5945), interaction (F2,38 = 0.58, P = 0.5625).
3J	N = 5, drinking days: N = 30 (5 excl: 2 technical errors, 2 with <2 bouts)	Simple linear regression: R = 0.445, *P = 0.0257.
3K	Bouts: total mice: N = 5, low E2 status days: N = 15 (excl, 1 bouts > 30 in a 30 min period, 1 technical error), high E2 status days: N = 15 (2 excl, 1 bouts > 30 in a 30 min period, 1 technical error); Normalized GCaMP signal: N = 5, low E2 days = 15, high E2 days = 15	Bouts (left): 2xRM-ANOVA: Epoch (F1,24 = 28.99, ****P < 0.0001), Estrous (F1,24 = 0.31, P = 0.5836), interaction (F1,24 = 7.05, *P = 0.0139). Post hoc paired t-tests with Holm-Sidak corrections between H2O and EtOH within group (low E2: t24 = 1.93, &P = 0.0656; high E2: t24 = 5.69, ****P < 0.0001). Normalized GCaMP signal (right): 2xRM-ANOVA: Epoch (F1,28 = 9.22, **P = 0.0051), Estrous (F1,28 = 0.18, P = 0.6736), interaction (F1,28 = 2.19, P = 0.1502). Post hoc paired t-tests with Holm-Sidak corrections between H2O and EtOH within group (low E2: t28 = 1.10, P = 0.2801; high E2: t28 = 3.19, **P = 0.0069).
3L	Bouts: N = 5, low E2 days = 15 (4 excl, technical error), high E2 days = 15 (6 excl: 5 technical error, 1outlier w/ > 30 bouts); Normalized GCaMP signal: N = 5, low E2 days = 15 (4 excl, trace technical error), high E2 days = 15 (5 excl, trace technical error)	Bouts: 2xRM-ANOVA: Epoch (F1,18 = 3.86, P = 0.0651), Estrous (F1,18 = 1.29, P = 0.2706), interaction (F1,18 = 0.77, P = 0.3912). Normalized GCaMP: 2xRM-ANOVA: Epoch (F1,19 = 3.34, P = 0.0833), Estrous (F1,19 = 1.02, P = 0.3258), interaction (F1,19 = 0.02, P = 0.8772).
3Q	N = 5, W1: low E2 days = 15, high E2 days = 15; EtOH 1: low E2 days = 15, high E2 days = 15; EtOH 2: low E2 days = 11 (4 excl, technical error), high E2 days = 11 (4 excl, technical error); W2: low E2 days = 11 (4 excl, technical error), high E2 days = 11 (4 excl, technical error)	RM Mixed-effects model: estrous (F1,28 = 0.41, P = 0.5286), epoch (F3,66 = 9.60, ****P < 0.0001), interaction (F3,66 = 0.86, P = 0.4652). Post hoc paired t-tests with Holm-Sidak corrections between epochs within group: low E2 status (W1 vs EtOH 1: t66 = 3.16, *P = 0.0142; W2 vs EtOH 2: t66 = 0.87, P = 0.6396); high E2 status (W1 vs EtOH 1: t66 = 2.95, *P = 0.0176; W2 vs EtOH 2: t66 = 3.03, *P = 0.0170).

3R	N = 5, W1: low E2 days = 15, high E2 days = 15; EtOH 1: low E2 days = 15, high E2 days = 15; EtOH 2: low E2 days = 11 (4 excl, technical error), high E2 days = 11 (4 excl, technical error); W2: low E2 days = 11 (4 excl, technical error), high E2 days = 11 (4 excl, technical error)	RM Mixed-effects model: estrous ($F_{1,28}$ = 0.34, P = 0.5652), epoch ($F_{3,66}$ = 1.40, P = 0.2499), interaction ($F_{3,66}$ = 4.15, **P = 0.0094). Post hoc paired t-tests with Holm-Sidak corrections between epochs within group: low E2 status (W1 vs EtOH 1: t_{66} = 0.90, P = 0.9378; W2 vs EtOH 2: t_{66} = 0.00, P > 0.9999); high E2 status (W1 vs EtOH 1: t_{66} = 2.58, *P = 0.0480; W2 vs EtOH 2: t_{66} = 0.00, P > 0.9999).
s3D	N = 5, low E2 days = 15 (2 exc, trace technical error), high E2 days = 15	Unpaired t-test between low E2 status and high E2 status females (t_{26} = 0.04, P = 0.9664).
s3H	N = 5, W1 to EtOH 1 (right): low E2 = 15, high E2 = 15; EtOH 2 to W2 (left): low E2 = 11 (4 excl, tehcnical error), high E2 = 9 (6 excl, technical error)	W1 to EtOH 1: 2xRM-ANOVA: Epoch ($F_{1,28}$ = 32.84, ****P = < 0.0001), Estrous ($F_{1,28}$ = 4.58, *P = 0.0412), interaction ($F_{1,28}$ = 0.07, P = 0.7978). Post hoc paired t-tests with Holm-Sidak corrections between epochs (low E2: t_{28} = 4.24, ***P = 0.0004; high E2: t_{28} = 3.89, ***P = 0.0006). EtOH 2 to W2: 2xRM-ANOVA: Epoch ($F_{1,19}$ = 48.90, ****P < 0.0001), Estrous ($F_{1,19}$ = 1.22, P = 0.2841), interaction ($F_{1,19}$ = 0.04, P = 0.8414). Post hoc paired t-tests with Holm-Sidak corrections between epochs (low E2: t_{19} = 4.92, $P = 0.0002; high E2: t_{19} = 4.97, $P = 0.0002).
s3G	N = 5, low E2 days = 11 (3 excl, technical error); high E2 days = 12 (1 excl, technical error)	Simple linear regression: R = 0.445, *P = 0.0257.
s3I	N = 5, W1 to EtOH 1 (right): low E2 = 15, high E2 = 15; EtOH 2 to W2 (left): low E2 = 11 (4 excl, tehcnical error), high E2 = 9 (6 excl, technical error)	W1 to EtOH 1: 2xRM-ANOVA: Epoch ($F_{1,28}$ = 6.83, *P = 0.0143), Estrous ($F_{1,28}$ = 0.06, P = 0.8036), interaction ($F_{1,28}$ = 7.53, *P = 0.0105). Post hoc paired t-tests with Holm-Sidak corrections between epochs (low E2: t_{28} = 0.09, P = 0.9266; high E2: t_{28} = 3.79, **P = 0.0015). EtOH 2 to W2: 2xRM-ANOVA: Epoch ($F_{1,18}$ = 8.49, **P = 0.0093), Estrous ($F_{1,18}$ = 1.25, P = 0.2777), interaction ($F_{1,18}$ = 0.09, P = 0.7678). Post hoc paired t-tests with Holm-Sidak corrections between epochs (low E2: t_{18} = 0.09, $P = 0.0546; high E2: t_{18} = 3.79, $P = 0.0950).
s3J	Low E2: N = 5 (1 mouse did not enter open arms), high E2: N = 6	Left: percent time in open arms: unpaired t-test between low E2 status and high E2 status females (t_9 = 1.93, &P = 0.0857); distance traveled: unpaired t-test between low E2 status and high E2 status females (t_9 = 0.52, P = 0.6143). Right: RM Mixed-effects model: compartment ($F_{2,17}$ = 6.48, **P = 0.0081), estrous ($F_{1,9}$ = 1.14, P = 0.3133), interaction ($F_{2,17}$ = 0.44, P = 0.6526). Post hoc paired t-tests with Holm-Sidak corrections between compartments within group: low E2 status (closed arms vs open arms: t_{17} = 2.09, P = &0.0579; closed arms vs center: t_{17} = 1.23, P = 0.4147; open arms vs center: t_{17} = 1.76, P = 0.3314); high E2 status (closed arms vs open arms: t_{17} = 2.05, P = 0.2490; closed arms vs center: t_{17} = 0.35, P = 0.7323; open arms vs center: t_{17} = 1.71, P = 0.3314).

s3K	Low E2: N = 4, high E2: N = 6	Left: percent time in center: unpaired t-test between low E2 status and high E2 status females (t8 = 1.91, &P = 0.0927); distance traveled: unpaired t-test between low E2 status and high E2 status females (t8 = 0.11, P = 0.9160). Right: 2xRM-ANOVA: compartment (F2,16 = 6.98, **P = 0.0066), estrous (F1,8 = 1.02, P = 0.3432), interaction (F2,16 = 0.08, P = 0.9219). Post hoc paired t-tests with Holm-Sidak corrections between compartments within group: low E2 status (walls vs corners: t16 = 0.66, P = 0.5158; walls vs center: t16 = 1.90, P = 0.1447; corners vs center: t16 = 2.57, &P = 0.0607); high E2 status (walls vs corners: t16 = 0.80, P = 0.4356; walls vs center: t16 = 1.78, P = 0.1779; corners vs center: t16 = 2.58, &P = 0.0587).
4B	VEH: N = 17 (4 excl, VEH drinking < 1 g/kg) , LET: N = 17 (2 excl, matched VEH exclusion mice)	Unpaired t-test between VEH and LET treatment (t30 = 3.81, ***P = 0.0006).
4C	VEH: N = 16 (1 excl, fell off maze), LET: N = 15 (1 excl, fell off maze)	Percent time in open arms: unpaired t-test between VEH and LET treatment (t27 = 0.09, P = 0.9309); distance traveled: unpaired t-test between VEH and LET treatment (t27 = 0.16, P = 0.8704).
4D	VEH: N = 6 (1 excl, experimentor error), LET: N = 6	1 hr DID: unpaired t-test between VEH and E2 treatment (t10 = 0.45, P = 0.6614); 2 hr DID: unpaired t-test between VEH and E2 treatment (t10 = 0.42, P = 0.6850).
4F	VEH: N = 8, E2: N = 8 (1 excl, miss)	1 hr DID: unpaired t-test between VEH and E2 treatment (t13 = 3.53, P = **0.0037); 2 hr DID: unpaired t-test between VEH and E2 treatment (t13 = 2.90, *P = 0.0125).
4G	VEH: N = 13 (1 excl, VEH drinking < 1 g/kg), mem-E2: N = 13 (2 excl, misses)	1 hr DID: unpaired t-test between VEH and E2 treatment (t21 = 2.46, P = *0.0227); 2 hr DID: unpaired t-test between VEH and E2 treatment (t21 = 1.74, &P = 0.0968).
4H	VEH: N = 8 (1 excl, miss), E2: N = 9 (1 excl, miss)	Percent time in open arms: unpaired t-test between VEH and E2 treatment (t13 = 0.55, P = 0.5059); distance traveled: unpaired t-test between VEH and E2 treatment (t13 = 0.13, P = 0.8986).
4K	0.01 nM E2: N = 2, n = 2 cells; 1 nM E2: N = 4, n = 4 cells; 10 nM E2: N = 5, n = 8 cells (1 excl, high degree of fluctuation in baseline), 100 nM E2: N = 4, n = 4 cells, 1000 nM E2 application: N = 3, n = 5 cells , 100 nM mE2: N = 3, n = 6 cells	2xRM-ANOVA: category (frequency vs amplitude; F1,44 = 2.70, P = 0.1075), E2 dose (F5,44 = 1.32, P = 0.2712), interaction (F5,44 = 0.81, P = 0.5430).
4L	N = 17 mice, n = 22 cells (17 increase, 5 no increase in freq; 7 increase,15 no increase in amp)	Fisher's exact test (P = **0.0058).
s5A	VEH: N = 17 (1 excl, VEH drinking < 1 g/kg), LET: N = 19	Unpaired t-test between VEH and LET treatment (t33 = 0.64, P = 0.5262).
s5B	VEH: N = 10, LET: N = 8	Unpaired t-test between VEH and LET treatment (t16 = 0.32, P = 0.7521).
s5C	Low E2: VEH: N = 13, LET: N = 12; hight E2: VEH: N = 9, LET: N = 10	Low E2: unpaired t-test between VEH and LET treatment (t23 = 1.44, P = 0.1627); high E2: unpaired t-test between VEH and LET treatment (t17 = 1.04, P = 0.3126).
s5D	VEH: N = 9, LET: N = 9	Percent time in open arms: unpaired t-test between VEH and LET treatment (t16 = 0.01, P = 0.9912); distance traveled: unpaired t-test between VEH and LET treatment (t16 = 1.36, P = 0.1922).

s6D	0.01 nM E2: N = 2, n = 2; 1 nM E2: N = 4, n = 4 cells; 10 nM E2: N = 5, n = 8 cells (1 excl, unstable baseline), 100 nM E2: N = 4, n = 4 cells, 1000 nM E2 application: N = 3, n = 5 cells	Frequency: simple linear regression: R = 0.03, P = 0.8835; amplitude: simple linear regression: R = 0.42, P = 0.0516.
5D	N = 4	2xRM-ANOVA: receptor ($F_{1,3}$ = 36.64, **P = 0.0090), CRF status ($F_{1,3}$ = 9.74, P = 0.0524), interaction ($F_{1, 3}$ = 3.90, P = 0.1428). Post hoc paired t-tests with Holm-Sidak corrections between ERα and ERβ: CRF+ (t_3 = 11.98, **P = 0.0025); CRF- (t_3 = 9.19, **P = 0.0054). Post hoc paired t-tests with Hold-Sidak corrections between CRF+ and CRF-: ERα (t_6 = 3.64, *P = 0.0216); ERβ (t_6 = 2.13, &P = 0.0775).
5E	N = 4	2xRM-ANOVA: receptor ($F_{1,3}$ = 26.81, *P = 0.0140), vGLUT2 status ($F_{1,3}$ = 15.71, *P = 0.0287), interaction ($F_{1,3}$ = 18.72, *P = 0.0228). Post hoc paired t-tests with Holm-Sidak corrections between ERα and ERβ: vGLUT2+ (t_3 = 8.18, **P = 0.0076); vGLUT2- (t_3 = 2.06, P = 0.2463). Post hoc paired t-tests with Hold-Sidak corrections between vGLUT2+ and vGLUT-: ERα (t_6 = 5.65, **P = 0.0026); ERβ (t_6 = 1.08, P = 0.3211).
5H	N = 4 mice, n = 7 cells (frequency: 1 increase, 1 variable change, 5 decrease; ampltiude: 1 increase, 2 decrease, 4 no change)	One sample t-test: frequency (increase: too few points; variable: too few points; decrease: t_4 = 6.99, **P = 0.0022); amplitude (increase: too few points; decrease: t_1 = 4.99, P = 0.1259; no change: t_3 = 1.10, P = 0.3522).
5J	VEH: N = 11 (3 excl, 2 misses, 1 no dye/damage), MPP: N = 11 (3 excl, 2 misses, 1 no dye/damage); VEH: N = 9 (2 excl, 1 miss, 1 no dye/damage), PHTPP = 9 (2 excl, 1 miss, 1 no dye/damage)	MPP: paired t-test between VEH and MPP treatment (t_7 = 2.93, *P = 0.0221); PHTPP: paired t-test between VEH and PHTPP treatment (t_6 = 1.05, P = 0.3346)
5K	VEH: N = 8, MPP: N = 8 (1 excl, mouse died before histology)	Percent time in light: unpaired t-test between VEH and MPP treatment (t_{13} = 0.77, P = 0.4526); distance in light: upaired t-test between VEH and MPP treatment (t_{13} = 1.41, P = 0.1810)
5L	VEH: N = 6 (1 excl, mouse died before histology), PHTPP: N = 6	Percent time in center: unpaired t-test between VEH and PHTPP treatment (t_9 = 0.08, P = 0.9369); distance in light: upaired t-test between VEH and PHTPP treatment (t_9 = 0.98, P = 0.3545)
s7I	N = 3 mice, n = 7 cells (frequency: 1 increase, 1 variable change, 2 decrease, 3 no change; ampltiude: 1 increase, 6 no change)	One sample t-test: frequency (increase: too few points; variable: too few points; decrease: t_1 = 5.74, P = 0.1097; no change: t_2 = 0.29, P = 0.7964); amplitude (increase: too few points; no change: t_5 = 0.10, P = 0.9249).
s7K	VEH: N = 6, MPP: N = 6	Paired t-test between VEH and MPP treatment (t_7 = 0.65, P = 0.5375).

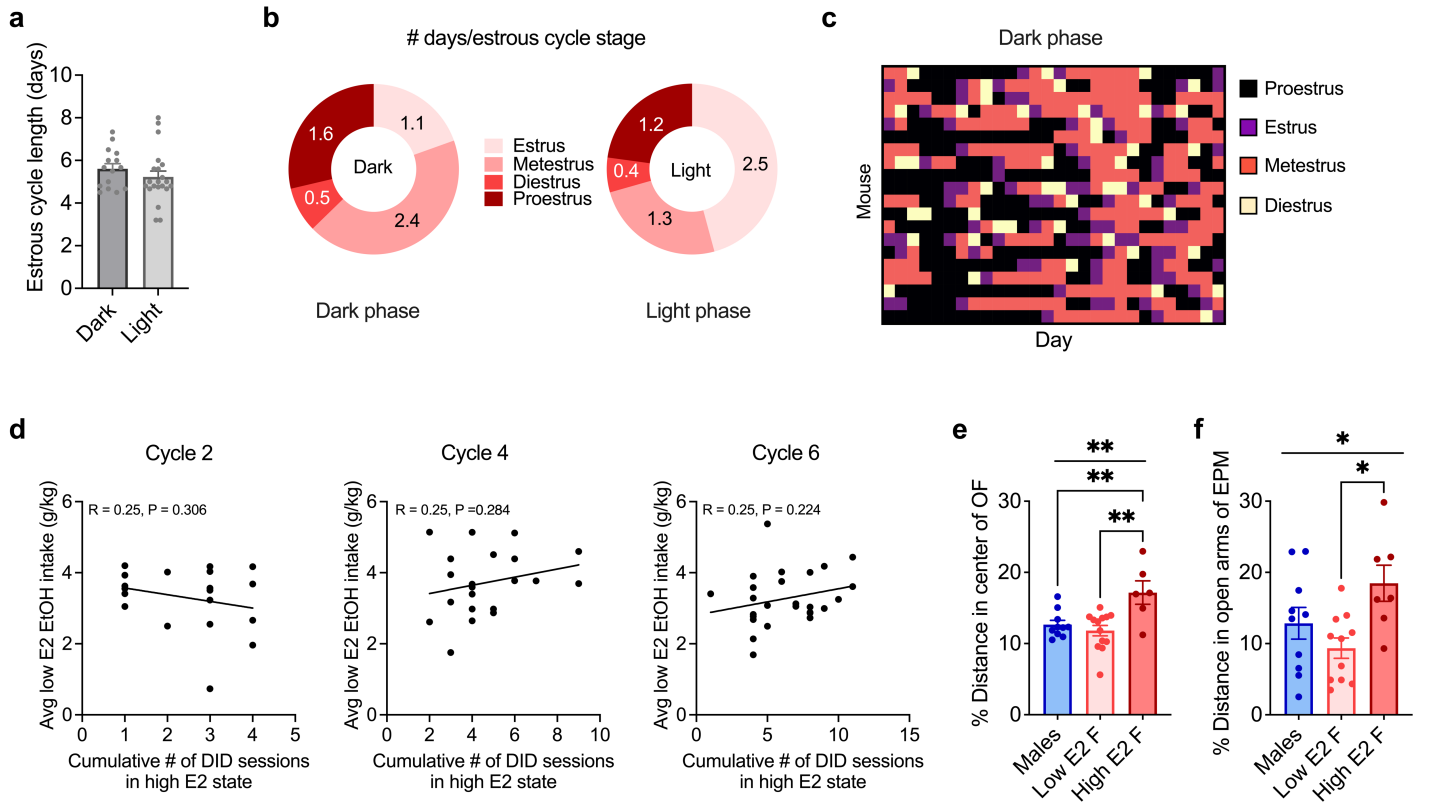

Extended data Figure 1: Estrous cycle determined by vaginal cytology during the light and dark phases of the light-dark cycle (related to Fig. 1). a–c) Estrous cycle monitoring in naïve female mice in **Fig. 1b-c**. **a)** Average estrous cycle length of individual naïve female mice as measured by vaginal cytology daily 2 hour into was not different in dark vs. 2 hours into the light phase of the light-dark cycle. **b)** Pie charts showing the average distribution of estrous cycle stages of mice in **a**. **c)** Heat map showing estrous cyclicity of individual mice across three weeks of tracking during the dark phase of the light-dark cycle, with each row representing one mouse and each color-coded cell on the x-axis representing estrous cycle stage on that day. Estrous cycle becomes stable across the first several weeks and then remains stable for months. **d)** The number of cumulative EtOH drinking days in a high ovarian E2 state did not affect subsequent drinking levels in a low ovarian E2 state at any point. **e-f)** % Distance traveled in the center of the open field (OF; **e**) and in the open arms of the elevated plus maze (EPM; **f**) are consistent with % time spent in these compartments shown in **Fig. 1i,l**. *P < 0.05, **P < 0.01; one way ANOVA main effects of group, post hoc t-tests with H-S corrections as indicated. Detailed statistics are provided in **Supplemental Table 1**.

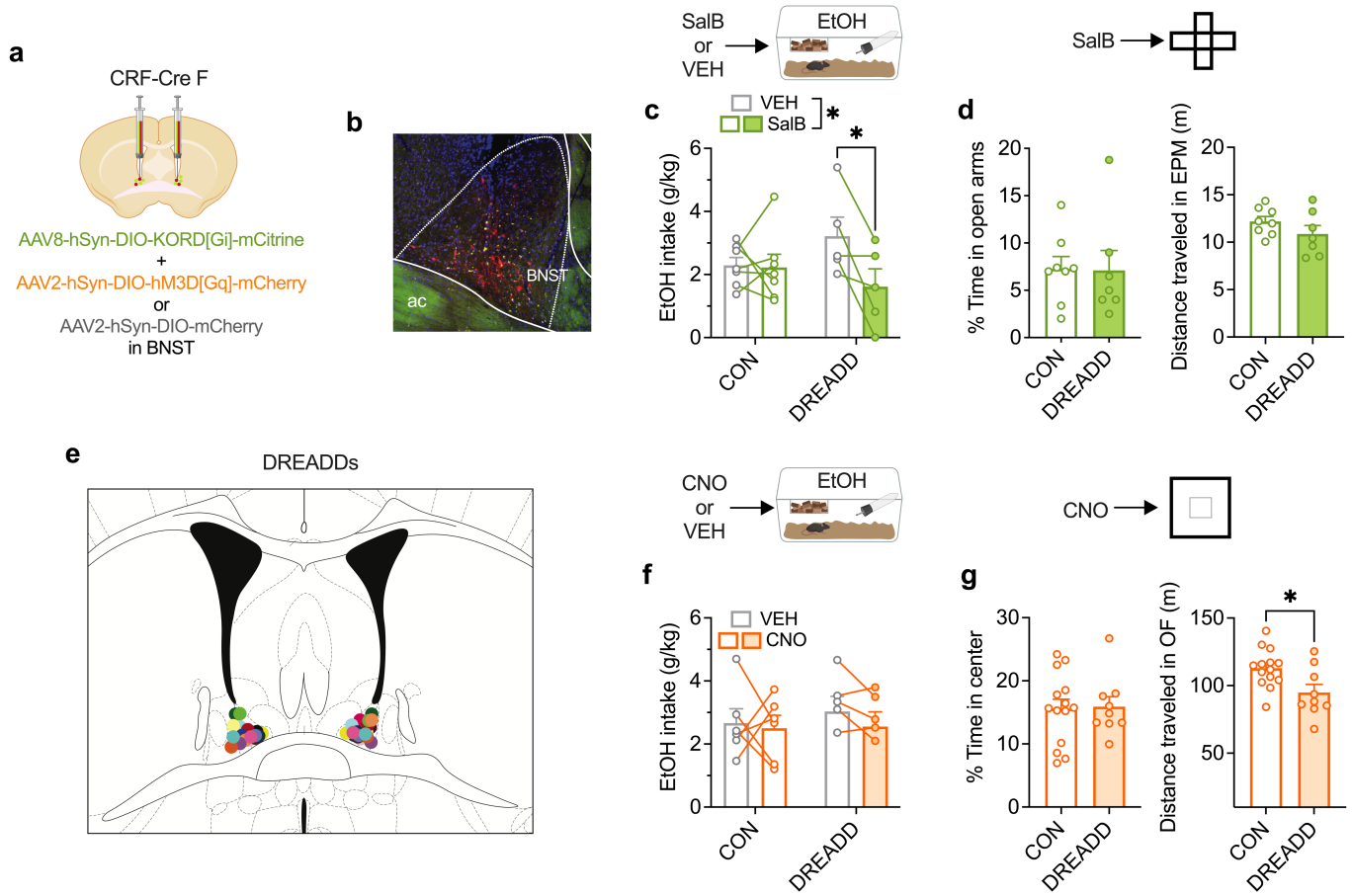

Extended data Figure 2: BNST^{CRF} neurons are necessary for binge alcohol consumption. a-g) Chemogenetic manipulation of BNST^{CRF} neurons during EtOH Drinking in the Dark (DID) and avoidance behaviors. **a-b)** Schematic (**a**) and representative image (**b**) for viral strategy to bidirectionally manipulate BNST^{CRF} neurons using a multiplexed Gi+Gq DREADD approach. **c-d)** Activation of the Gi-coupled KOR DREADD via systemic injection of Salvinorin B (SalB; 10 mg/kg) suppressed binge EtOH consumption compared to vehicle (VEH) injected controls (**c**) but did not affect the % time in open arms of the elevated plus maze (EPM; left) or distance traveled (right; **d**). **e)** DREADD virus hit map in the BNST (for **Fig. 2a**–**f**). Each dot is an individual hit and the grey Xs are a miss. **f-g)** Gq DREADD-mediated BNST^{CRF} neuron activation via clozapine-N-oxide (CNO; 5 mg/kg i.p.) did not change EtOH consumption (**f**) or alter avoidance behavior on the open field (OF) measured via % time in center (left) but did reduce distance traveled (right; **g**).*P < 0.05, unpaired t-tests between CON and DREADD; 2xANOVA main effects and interactions between groups and treatment; post hoc t-tests with H-S corrections as indicated. Detailed statistics are provided in **Supplemental Table 1**. Illustrations were created with biorender.com.

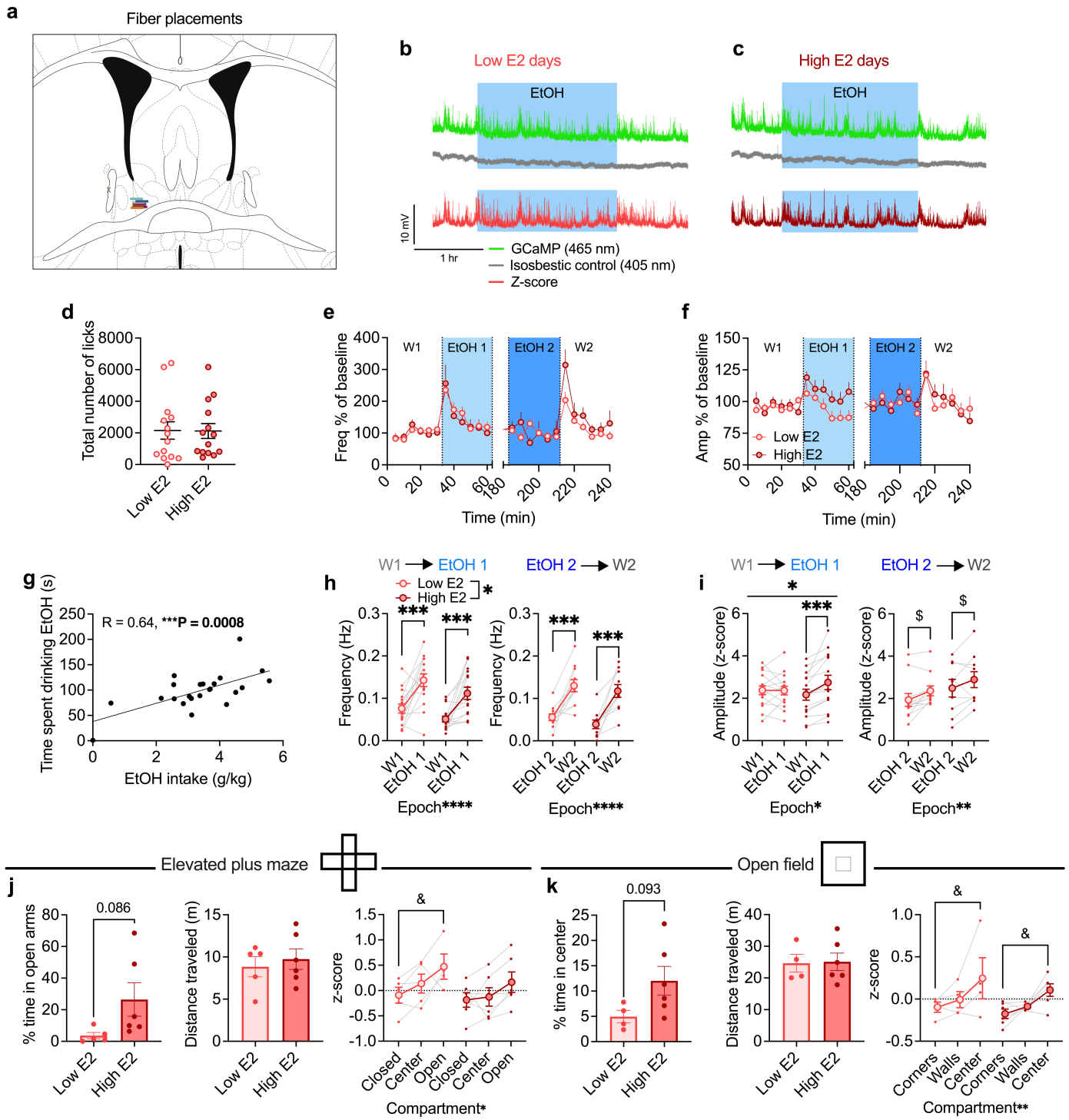

Extended data Figure 3: Fiber photometry additional measures (related to Fig. 3). a) Hit map of fiber photometry cannulae in the BNST. Each line corresponds to the fiber placement and the grey X corresponds to a surgical miss that was not used in experiments due to poor GCaMP signal. **b)** Fiber photometry signals in the 465 nm excitation (GCaMP), isobestic 405 nm (control) wavelength channels, and normalized z-score during EtOH-DID in low E2 status and high E2 status female drinking days (**c**). **d)** There was no difference in total licks (TTLs) across epochs between low E2 and high E2 status drinking days. **e)** Time course of transient event frequency as a % of W1 baseline across the 30 minutes of W1, first 30 minutes of EtOH (EtOH 1), last 30 minutes of EtOH (EtOH 2), and the first 30 minutes of W2 in 5 minutes bins. **f)** Time course of transient event peak amplitudes as a % of W1 baseline across the 30 minutes of W1, EtOH 1, EtOH 2, and the first 30 minutes of W2 in 5 minutes bins. **g)** There was a positive correlation between time spent drinking EtOH (s) and g/kg EtOH intake during the EtOH epoch. **h)** There was an increase in transient event frequency during low and E2 status drinking days during the transition from the last 5 minutes of W1 to EtOH 1 (left) and the last 5 minutes of EtOH 2 and W2 (right). **i)** There was an increase in transient event amplitude in the first 5 minutes of EtOH 1 compared to the last 5 minutes of W1during high E2 status drinking days but not during low E2 status drinking days (left), with no change during the transition

from EtOH 2 to W2 (right). **j)** There was a trend towards increased % time spent in the open arms of the elevated plus maze (EPM) on high E2 status days compared to low E2 status days (left), with no change in distance traveled (center), and a trend towards increased normalized GCaMP signal in the open arms compared to the closed arms of the EPM on low E2 status days but not high E2 status days (right). **k)** There was a trend towards increased % time spent in the center of the open field (OF) on high E2 status days (left), with no effect on distance (center), and a trend towards increased normalized GCaMP signal in the center compared to the corners of the OF on low and high E2 status days (right). *P < 0.05, **P < 0.01, ***P < 0.001, ****P < 0.0001; unpaired t-tests between low vs high E2; 2xANOVA main effects and interactions between groups and time/compartment; post hoc t-tests with H-S corrections as indicated. $P < 0.10 for post hoc t-tests with H-S corrections between groups. Detailed statistics are provided in **Supplemental Table 1**.

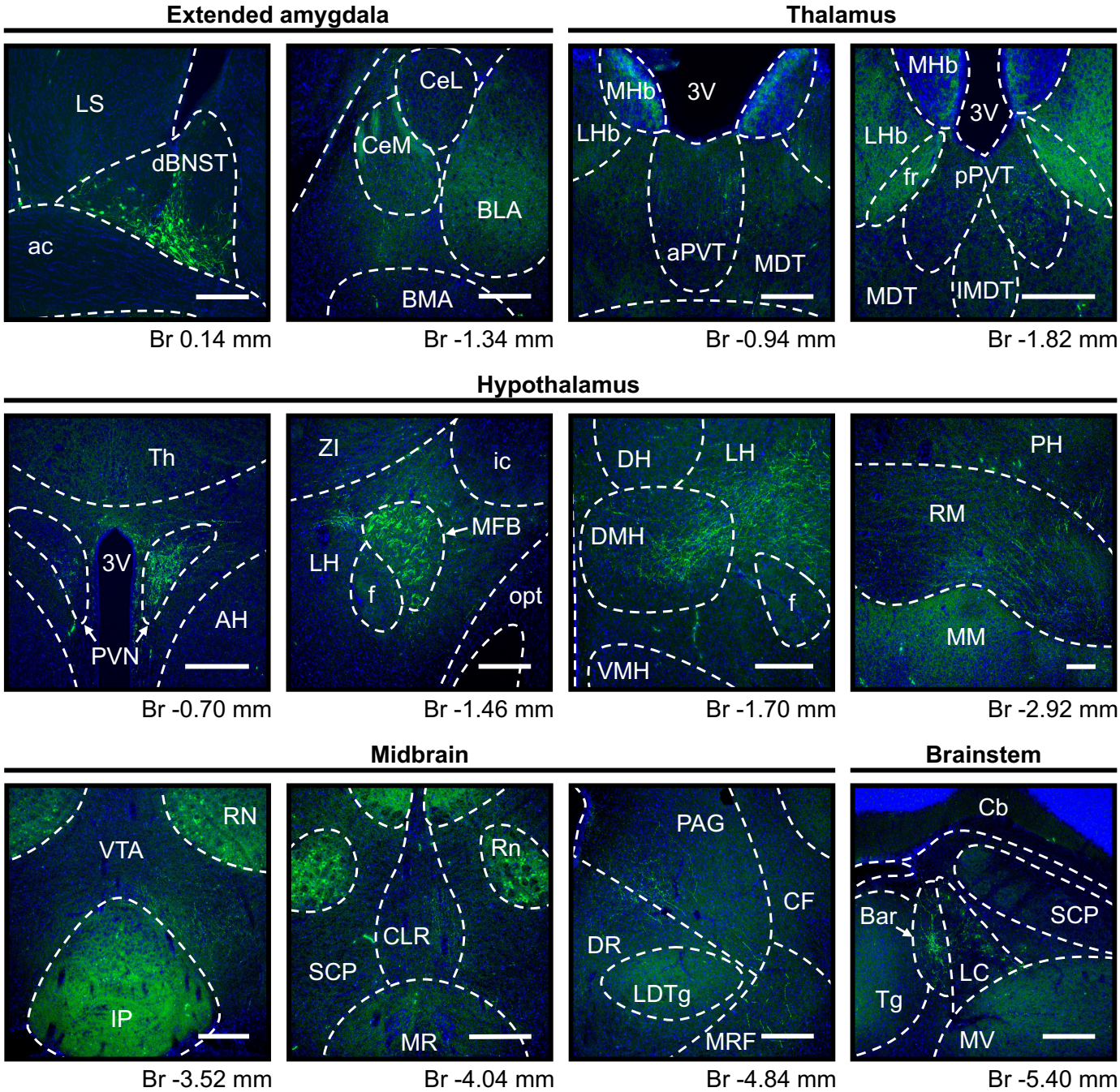

Extended data Figure 4. BNST^{CRF} neuron projections (GCaMP tracing; related to Fig. 3). Female BNST^{CRF} neuron projection targets in the extended amygdala, thalamus, hypothalamus, midbrain, and brainstem. Abbreviations: 3V - 3rd ventricle, ac - anterior commissure, AH - anterior hypothalamic area, aPVT - paraventricular thalamic nucleus, anterior part, Bar - Barrington's nucleus, BLA - basolateral amygdala, BMA - basomedial amygdala, Cb - cerebellum, CeL - central amygdala, lateral division, CeM - central amygdala, medial division, CF - cuneiform nucleus, CLR - caudal linear nucleus of the raphe, dBNST - bed nucleus of stria terminalis, dorsal part, DMH - dorsomedial hypothalamic nucleus, DH - dorsal hypothalamic area, DR - dorsal raphe nucleus, f - fornix, fr - fasciculus retroflexus, ic - internal capsule, IMDT - intermediodorsal thalamic nucleus, IP - interpeduncular nucleus, LC - locus coeruleus, LDTg - laterodorsal tegmental nucleus, LH - lateral hypothalamus, LHb - lateral habenular nucleus, LS - lateral septal nucleus, MDT - mediodorsal thalamic nucleus, MDT - mediodorsal thalamic nucleus, MFB - medial forebrain bundle, MHb - medial habenular nucleus, MM - medial mammillary nucleus, MR - median raphe nucleus, MRF - mesencephalic reticular formation, MV - medial vestibular nucleus, opt - optic tract, PAG - periaqueductal gray, PH - posterior hypothalamic nucleus, pPVT - paraventricular thalamic nucleus, posterior part, PVN - paraventricular hypothalamic nucleus, RM - retromammillary nucleus, RN - red nucleus, SCP - superior cerebellar peduncle, Tg - tegmental nucleus, Th - thalamus, VMH - ventromedial hypothalamic nucleus, VTA - ventral tegmental area, ZI - zona incerta.

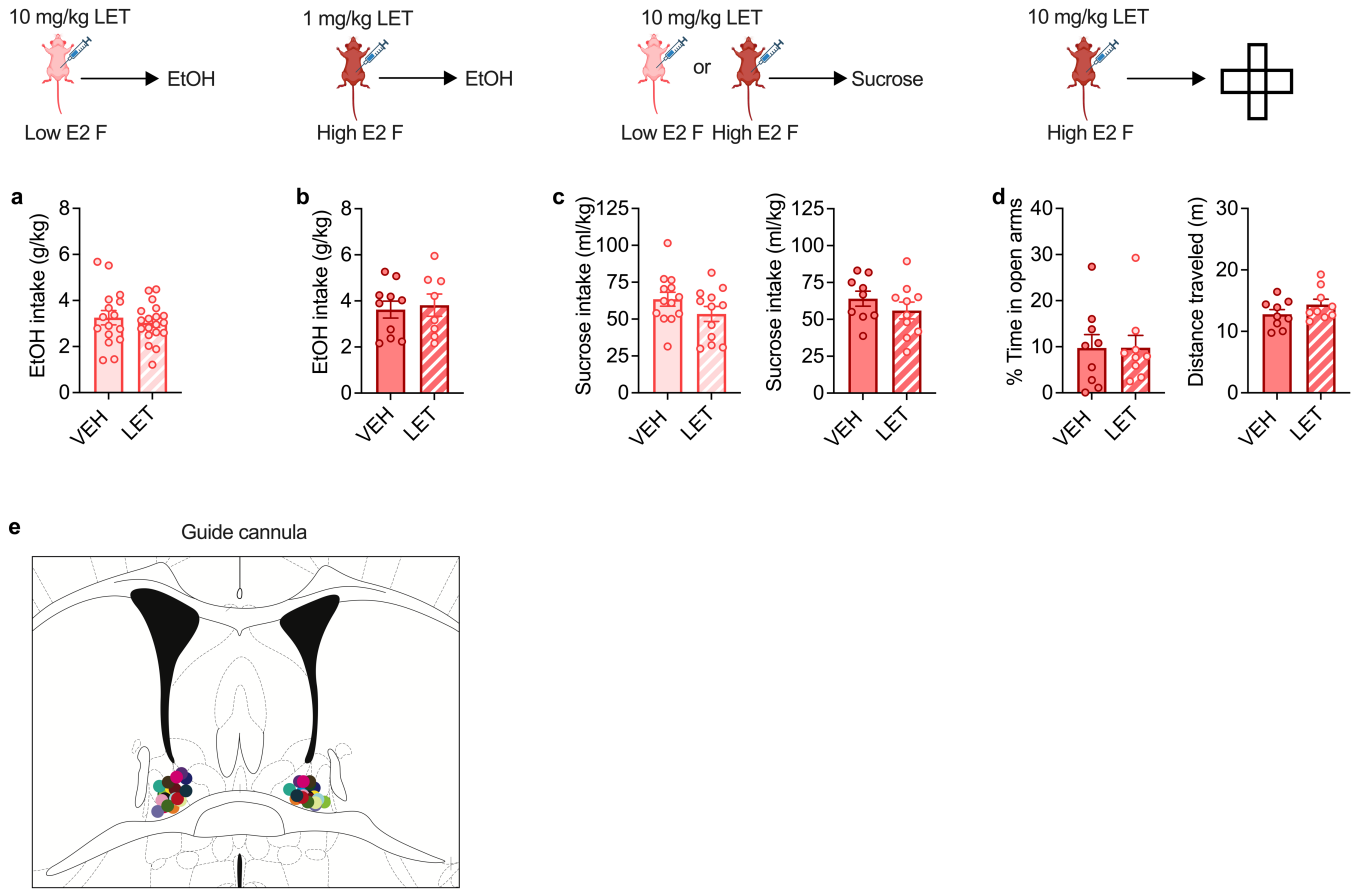

Extended data Figure 5: Effects of rapid E2 signaling on binge alcohol consumption, binge sucrose consumption, and avoidance behavior are dose- and ovarian E2 state-dependent (related to Fig. 4). a-d) Behavioral effects of systemic estrogen synthesis inhibition using acute systemic administration of letrozole (LET) given 40 minutes prior to behavioral testing in high or low E2 status females. **a)** Acute LET (10 mg/kg i.p.) did not alter binge EtOH consumption in low E2 status females. **b)** Acute systemic administration of a low dose of LET (1 mg/kg, i.p.) did not alter binge EtOH consumption in high E2 status females, while a high dose of LET did (**Fig. 4**). **c)** Acute systemic LET (10 mg/kg, i.p) did not alter binge sucrose consumption in females in either a low ovarian E2 state (left) or high ovarian E2 state (right). **d)** Acute LET administration in high E2 status females 2 hours prior to EPM did not alter the % time spent in the open arms (left) or distance traveled (right). **e)** BNST guide cannulae placements following histology (for **Fig. 4f-i**); each dot is an individual hit. Detailed statistics are provided in Supplemental Table 1. Illustrations were created with biorender.com.

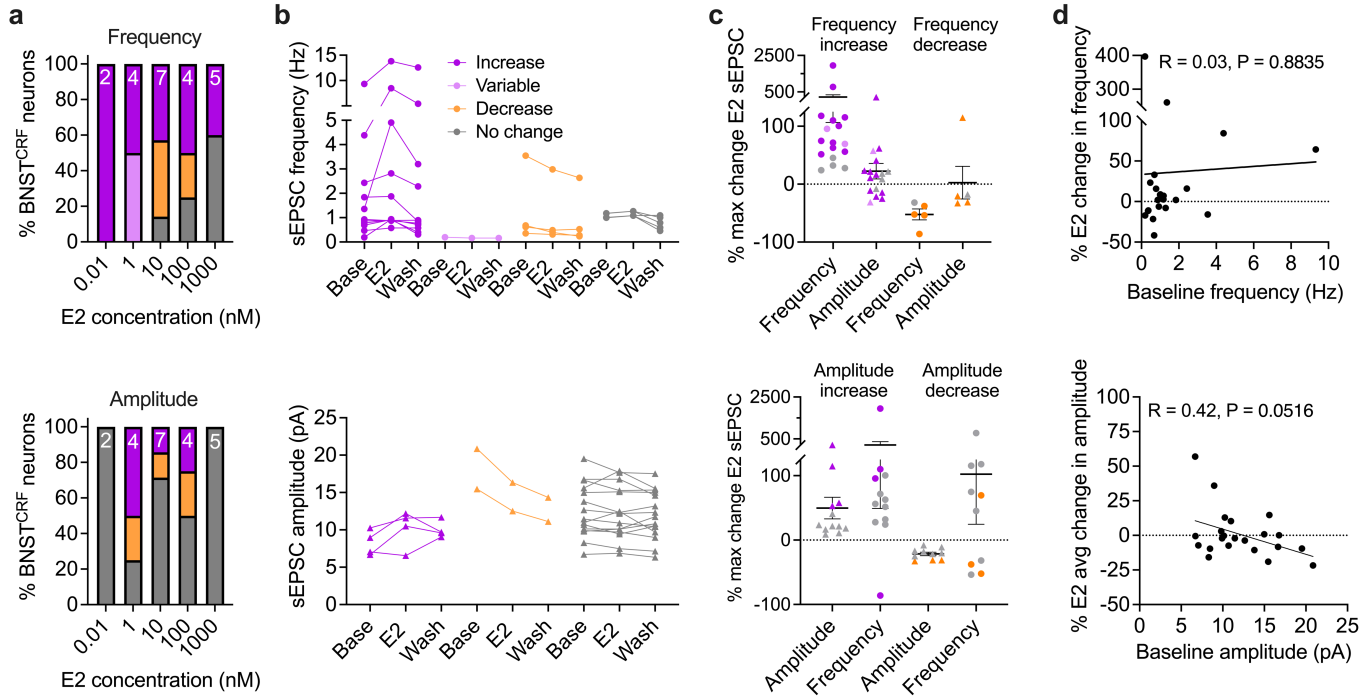

Extended data Figure 6: E2 sEPSC frequency responsive BNST^{CRF} cells have a specific cellular phenotype (related to Fig. 4). a) Proportion of responder categories during 10-minute E2 wash on across E2 doses (0.01, 1, 10, 100, 1000 nM) for frequency (top) and amplitude (bottom). **b)** Raw average frequency (top) and amplitude (bottom) during baseline, E2 wash on, and washout for each cell. **c)** Maximum % change from baseline for cells categorized as increased and decreased during E2 wash on for frequency (top) and amplitude (bottom). Amplitude did not differ between BNST^{CRF} neurons that had increased vs. decreased frequency (top) and vice versa (bottom). **d)** % change from baseline in frequency (top) and amplitude (bottom) during E2 did not correlate with baseline frequency and amplitude. Detailed statistics are provided in Supplemental Table 1.

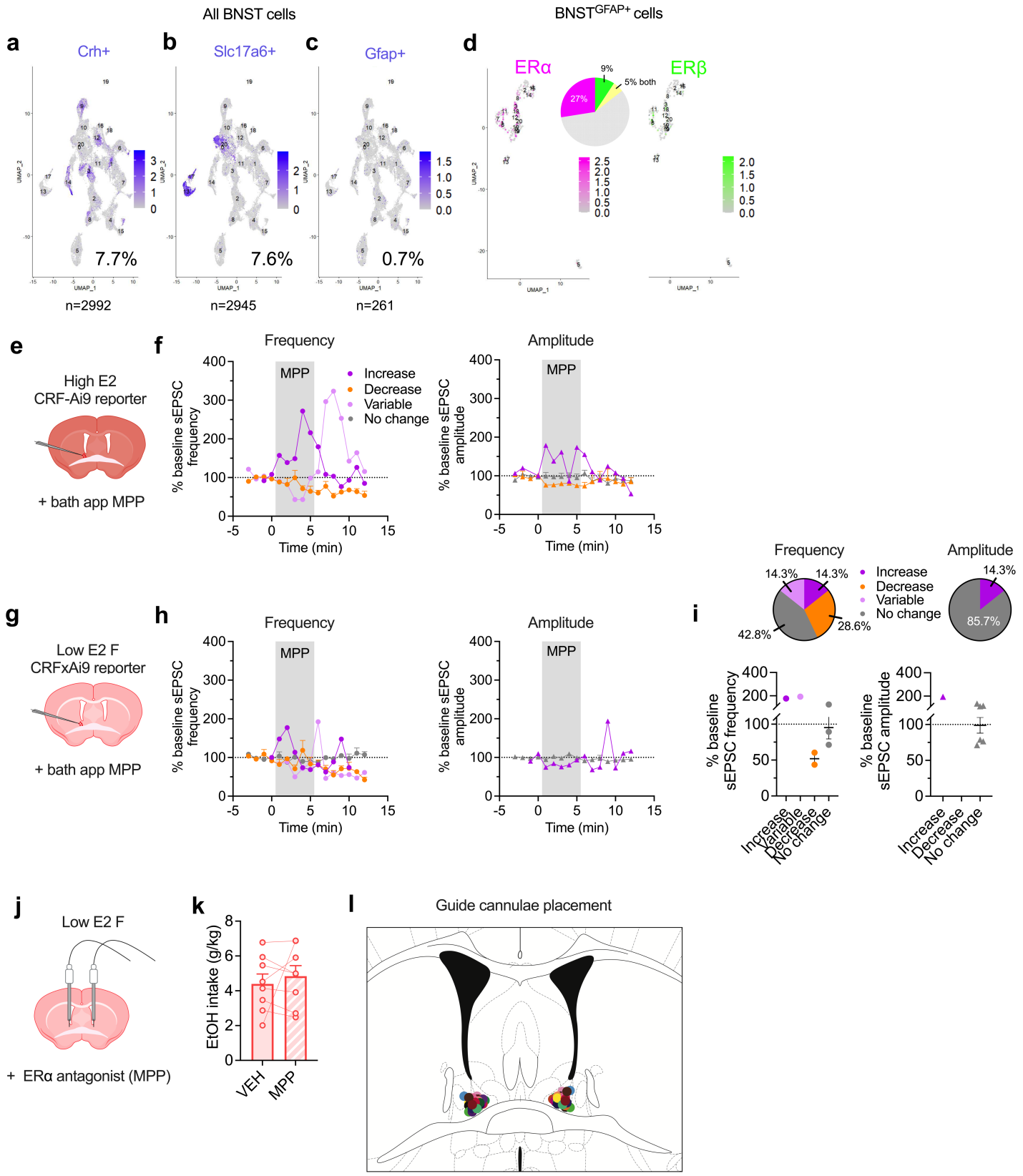

Extended data Figure 7: BNST cell population analysis, MPP pharmacology (*ex vivo* slice electrophysiology and *in vivo* intra-BNST infusion; related to Fig. 5). a-d) Analysis of single nucleus RNA sequencing of female BNST nuclei (total cells: 38,806; GEO: GSE126836)[78]. **a)** *Crh* (CRF) expression (7.7%) in female BNST cells. **b)** *Slc117a6* (VGLUT2) expression (7.6%) in female BNST cells. **c)** *Gfap* (GFAP) expression (0.7%) in female BNST cells. **d)** ERα (27%) and ERβ (9%) expression (5% both) in female BNST^{GFAP} cells. **e-f)** Effects of acute bath application of the ERα antagonist methyl-piperidino-pyrazole (MPP) on excitatory synaptic transmission in BNST^{CRF} neurons during whole-cell slice electrophysiology

recordings in high ovarian E2 female CRF-CrexAi9 reporter mice, as depicted in **e**. **f)** Time course of high E2 status $BNST^{CRF}$ neurons that displayed an increase, decrease, or variable change in spontaneous excitatory postsynaptic current (sEPSC) frequency (left) and amplitude (right) % change from baseline during the 5-minute MPP wash on application period and 5 minute washout. **g-i)** Effects of acute bath application of MPP on excitatory synaptic transmission in $BNST^{CRF}$ neurons during whole-cell slice electrophysiology recordings in low ovarian E2 female CRF-CrexAi9 reporter mice, as depicted in **g**. **f)** Time course of low E2 status $BNST^{CRF}$ neurons that displayed an increase, decrease, or variable change in spontaneous excitatory postsynaptic current (sEPSC) frequency (left) and amplitude (right) % change from baseline during the 5-minute MPP wash on application period and 5 minute washout. **i)** Bath application of MPP (3 μM) had no effect on spontaneous excitatory postsynaptic current (sEPSC) frequency (left) and amplitude (right) in a majority of cells during the 5 min wash on period. **j)** Depiction of strategy to site-deliver MPP (10 μM/200 nl/side or saline vehicle (VEH) to the BNST in low E2 females via bilateral indwelling cannulae 10 minutes prior to behavioral testing. **k)** ERα antagonism via intra-BNST MPP did not alter binge EtOH drinking in low ovarian E2 status females. **l)** BNST cannula hit map (for **Fig. 4d-e, 5j-l**); each dot is an individual hit. Detailed statistics are provided in **Supplemental Table 1**. Illustrations were created with biorender.com.

Acknowledgments

Funding
This research was supported by: NIH grants K99/R00 AA023559 and R01 AA027645, a NARSAD Young Investigator Award, a Stephen and Anna-Maria Kellen Foundation Junior Faculty Award 26608 (K.E.P.); NIH grant F31 AA029293 (L.J.Z.); NIH grant T32 DA039080 (J.K.R.I., L.J.Z., O.B.L.); National Institute of General Medical Sciences of the National Institutes of Health Medical Scientist Training Program grant to the Weill Cornell/Rockefeller/Sloan Kettering Tri- Institutional MD-PhD Program T32GM007739 (C.K.H.); Deutsche Forschungsgemeinschaft Walter Benjamin Fellowship 516215326 (P.B.); NIH grant P51 OD011092 (KMF, DWE).

Author contributions
KEP conceptualized all experiments, KEP and LJZ planned all methodology. LJZ, JKRI, PUH, IP, DL, JPW, ASRR, RB, JA, OBL, MJS, CKH, KMF, HM, SN, JM, PG, PB, AS, LVH, DWE performed and analyzed data. LJZ, JKRI, PUH, and KEP visualized all data. KEP, DWE, and JG. oversaw experiments. KEP and LJZ wrote the manuscript, and all authors edited and approved the final version of the manuscript.

Competing interests
Authors declare that they have no competing interests.

Data availability
All raw and analyzed data will be made publicly available and accession codes provided prior to publication.

Code availability
All custom code written in MATLAB, R, and Python will be publicly deposited on GitHub prior to publication.